AN INVESTIGATION INTO THE LOCALIZATION OF PEPTIDE-GOLD NANOPARTICLES IN AN *IN VITRO* AND *IN VIVO* COLORECTAL CANCER MODEL

By

Lynn Candice Cairncross

A minithesis submitted in fulfilment of the requirements for the degree of Baccalaureus Magister Scientiae (MSc) Nanoscience in the Department of Biochemistry and Microbiology, Nelson Mandela Metropolitan University

February 2015

Supervisor: Prof. S. Roux

Co-supervisor: Prof. M. Meyer

TABLE OF CONTENTS

ABSTRACT ..... **i**
KEYWORDS ..... **ii**
DECLARATION ..... **iii**
LIST OF ABREVIATIONS ..... **v**
LIST OF SYMBOLS ..... **vii**
LIST OF FIGURES ..... **viii**
LIST OF TABLES ..... **x**
CHAPTER ONE: LITERATURE REVIEW 1
1.1. General introduction 1
1.2. Background to colorectal cancer 2
1.3. The structure and function of the large intestine 2
1.4. Molecular bases of colorectal carcinogenesis 3
1.4.1. APC/β-catenin and Wnt signalling pathway 4
1.4.2. KRAS oncogene and the EGFR signalling pathway 5
1.4.3. p53 gene 5
1.4.4. Chromosome 18q21 and TGF- β pathway 5
1.5. Colorectal cancer pathogenesis 6
1.5.1. Chromosomal instability (CIN) pathway 6
1.5.2. Microsatellite instability (MSI) pathway 7
1.5.3. CpG island methylator phenotype (CIMP) pathway 7
1.6. Animal model for colorectal carcinogenesis 8
1.6.1. Dimethylhydrazine and Azoxymethane 8
1.6.2. Dextran sulphate sodium 10
1.6.3. AOM/DSS- induced carcinogenesis model 10
1.7. Colorectal cancer screening tools 11
1.7.1. Endoscopic screening 11
1.7.2. Biomarker screening 12
1.8. Colorectal cancer targeting peptides 14
1.8.1. Why peptides? 14
1.8.2. The identification of cancer specific peptides 14
1.9. Nanotechnology based- delivery systems 15

1.9.1. Gold nanoparticles....16
1.9.1.1. Gold nanoparticle optical properties....17
1.9.1.2. Gold Nanoparticle *in vivo* diagnostic applications....18
1.10. The uptake and distribution of gold nanoparticles....19
1.11. The analysis of gold nanoparticle uptake and distribution....23
1.12. High resolution transmission electron microscopy....23
1.13. Aims and objectives....25
1.14. Thesis Scope....26
CHAPTER TWO: METHODS AND MATERIALS....27
2.1. Materials and methods....27
2.2. Solutions and buffers....27
2.3. Gold nanoparticles and characterisation....28
2.3.1. High resolution transmission electron microscopy....28
2.3.2. Energy dispersive X-ray spectroscopy....29
2.3.3. Dynamic light scattering and zeta potential....29
2.4. *In Vitro* Studies....29
2.4.1. Routine cell culture maintenance....29
2.4.3. Storing and thawing of cell culture....30
2.4.4. Cell culture nanoparticle exposure....30
2.4.5. TEM cell preparation....30
2.4.5.1. Sample washing and harvesting....32
2.4.5.2. Fixation....32
2.4.5.3. Dehydration....32
2.4.5.4. Embedding in LR White resin....32
2.5. *In vivo* Studies....33
2.5.1. Ethical approval....33
2.5.2. Animal maintenance....33
2.5.3. Animals and experimental design....33
2.5.4. Induction of colorectal cancer....35
2.5.4.1. AOM/DSS method 1....35
2.5.4.2. AOM/DSS method 2....35
2.5.5. Sacrifice of rats....36
2.5.6. Tissue harvesting....38

2.5.7. TEM tissue preparation 38
2.5.8. Ultramicrotome methodology for sectioning ultrathin sections. 38
2.5.9. Statistical analysis 40
CHAPTER THREE: RESULTS AND DISCUSSION 41
3.1. Characterization of AuNPs 41
3.1.1. Aims of investigation 41
3.1.2. Results 41
3.1.2.1. Characterisation by high resolution transmission electron microscopy 41
3.1.2.2. Characterisation by dynamic light scattering and zeta potential 41
3.1.3. Discussion 43
3.2. *In vitro* studies 43
3.2.1. Aim of investigation 43
3.2.2. Results 44
3.2.3. Discussion 45
3.2.3.1. Cell harvesting 46
3.2.3.2. Fixation of cells 47
3.2.3.3. Dehydration and embedding of cells 48
3.2.3.4. Sectioning 49
3.3. *In vivo* studies 49
3.3.1. Aim of investigation 49
3.3.2. Results 50
3.3.2.1. The induction of colorectal cancer in rat model 50
3.3.2.2. HRTEM analysis of tissue 53
3.3.3. Discussion 60
CHAPTER FOUR: CONCLUSION AND FUTURE DIRECTIONS 63
4.1. Conclusion 63
4.2. Recommendations for future work 65
4.3. Limitations 65
BIBLIOGRAPHY **66**
APPENDIX **74**

ABSTRACT

Background: Colorectal cancer is the third most common cancer and cause of related deaths worldwide. Early colorectal cancer diagnosis is vital in reducing incidence and mortality. There is a need for the development of non-invasive screening tools for enhancing the detection of the disease. Cancer specific peptides are useful cancer targeting agents that can be used to specifically improve early detection strategies. Several cancer targeting peptides have been identified. Previous work investigated the specific binding of three of these peptides (p.C, p.L and p.14) conjugated to quantum dots and were found to bind to colorectal cancer cell lines (HT-29 and Caco-2). However, their uptake, localization and biodistribution in an *in vitro* and *in vivo* colorectal cancer model have not been determined. This is essential in gaining an understanding for future diagnostic or therapeutic based applications. **Primary Aim**: The aim of this study was investigate the localization of three selected peptides p.C, p.L and p.14 conjugated to gold nanoparticles in an *in vitro* and *in vivo* colorectal cancer model using HRTEM. **Methodology:** The AuNP/peptide conjugates were characterized by HRTEM and DLS. For *in vitro* studies; HT-29, Caco-2 and C3A cells were exposed to the AuNP-p.C, AuNP-p.L and AuNP-p.14, collected and processed for HRTEM to assess targeting and localization. For *in vivo* studies; the establishment of a colorectal cancer model using the AOM/DSS model 1 and 2 was conducted. Wistar rats were assigned to 6 groups, five experimental and 1 control group. Group 1 received AOM/DSS method 1 and was treated with AuNP-p.L. Group 2 and 3 received AOM/DSS method 2 and were treated with AuNP-p.C and AuNP-p.14. Group 4 and 5 remained healthy and treated with AuNP-p.C and AuNP-p.14. Group 6 remained healthy receiving no nanoparticle treatment. After treatment, rats were sacrificed and tissue was processed for HRTEM. Tissue chosen for HRTEM analysis included: Group 1 (inflamed colon, rectum, pancreatic and kidney), Group 4 (kidney) and Group 5 (liver). **Results:** results obtained from nanoparticle characterization suggested that nanoparticles were conjugated to their respective peptides and were stable in dispersion. For *in vitro* studies, results suggested no AuNP targeting and localization in HT-29 cell lines. For *in vivo* studies, no colorectal cancer tumours were induced. TEM micrographs did not indicate the presence of nanoparticles in colon, rectum, pancreatic, kidney and liver tissue. However, AuNPs were found in the kidney tissue (group 4). **Conclusion:** Although the overall objectives were not met, this study provided insight into TEM cell preparation and optimization for future nanoparticle cell interaction research. This study also demonstrated the absence of AuNPs in healthy tissue and the presence of AuNPs in healthy kidney tissue through renal clearance, a favourable quality for diagnostic or therapeutic applications

KEYWORDS

Colorectal Cancer

AOM/DSS Method

Early Detection

Biomarkers

Cancer Targeting Peptides

Conjugation

Nanotechnology

Gold Nanoparticles

High Resolution Transmission Electron Microscopy

Localization

DECLARATION

I, **Lynn Candice Cairncross (s209079436),** hereby declare that the dissertation for **Magister Scientiae (M.Sc.) Nanoscience** to be awarded is my own work and that it has not previously been submitted for assessment or completion of any postgraduate qualification to another University or for another qualification.

…….. (Signature)
Lynn Candice Cairncross

Official use:
In accordance with Rule G5.6.3,
5.6.3 A treatise/dissertation/thesis must be accompanied by a written declaration on the part of the candidate to the effect that it is his/her own work and that it has not previously been submitted for assessment to another University or for another qualification. However, material from publications by the candidate may be embodied in a treatise/dissertation/thesis

ACKNOWLEDGEMENTS

The author would like to express her appreciation to those who supported her throughout her development of her dissertation especially to:

- Prof. Saartjie Roux[1] (Supervisor), for your friendliness, guidance, time invested, patience you've shown me and you're encouraging words throughout my project.
- Prof. Mervin Meyer[2] (co-supervisor) for your assistance, knowledge and understanding throughout the duration of this project and proofreading my thesis.
- My family for your continuous support, encouragement, Love and guidance throughout my studies.
- To Calvin Kashorte for your encouragement.
- Dr. Ernest Fredericks[3] for his knowledge and expertise in Gastroenterology.
- Dr. Allen Hall[4] and team for their assistance and expertise.
- Professor Mike Lee, Dr.J.Olivier, Dr.A.Janse Van Vuuren[5] and HRTEM team for their knowledge and assistance
- I would also like to express my sincere gratitude to Nooreen Agherdien, Valencia Jamalie and Chyril Abrahams.
- To Disang Lekutlane, Maleeha Fortuin-Seedat and Chiuswa Chengetanai for your assistance whenever needed.
- MINTEK and Minpeptide for supplying me with peptide functionalized gold nanoparticles
- Nelson Mandela Metropolitan University for their financial assistance
- The National Nanoscience Teaching and Training Platform and the Department of Science and Technology (DST) for funding this project

[1] Department of Biochemistry and Microbiology, Nelson Mandela Metropolitan University, PO Box 77000, Port Elizabeth 6031, South Africa

[2] Department of Biotechnology, University of the Western Cape, Bellville, 7535, South Africa

[3] Netcare Greenacres Hospital, Greenacres, Port Elizabeth, Eastern Cape, South Africa

[4] Laboratory for Microscopy and Microanalysis, University of Pretoria, Natural Sciences Building II

[5] Centre of HRTEM, Nelson Mandela Metropolitan University, PO Box 77000, Port Elizabeth 6031, South Africa

LIST OF ABREVIATIONS

AOM	azoxymethane
APC	adenomatous polyposis
AuNP	gold nanoparticle
AuNPs	gold nanoparticles
BF	bright field
CA 19-9	carbohydrate antigen 19-9
CANSA	Cancer Association of South Africa
CCSA-2,3 and 4	colon cancer-specific antigen-2,3,4
CEA	carcinoembryonic antigen
CIMP	CpG island methylator phenotype
CIN	chromosome instability
CME	clathrin-mediated endocytosis
CRC	colorectal cancer
CT scan	computed tomography scan
CvME	caveolae-mediated endocytosis
DCC	deleted in colon cancer
DcR3	death decoy receptor-3
DF	dark Field
dH2O	deionized water
DLS	dynamic light scattering
DMEM	dulbecco's modified eagle's medium
DMH	dimethylhydrazine
DNA	deoxyribonucleic acid
DSS	dextran sulfate sodium
EGFR	epidermal growth factor receptor
EMEM	eagles minimum essential medium
EPR	enhance permeability and retention
FAP	familial adenomatous
FOBT	faecal occult blood test
GDP	guanosine diphosphate
GIT	gastrointestinal tract
GSK-3β	glycogen synthase-3β
GTP	guanosine-5'-triphosphate
HAADF	High angle annular dark field
HD	hydrodynamic diameter
HNPCC	hereditary non-polyposis colorectal cancer
HRTEM	high resolution transmission electron microscopy
iNOS-2	nitric-oxide synthase
IV	intravenous route

K-ras	kirstin ras
LOH	loss of heterozygosity
MAM	methylazoxymethanol
MIF	macrophage migration inhibitory factor
MLH1,3	MutS homolog 1,3
MMP-7,9	matrix metallopeptide-7,9
MMR	mismatch repair mechanism
MRI	magnetic resonance imaging
MSH2, 6	MutS homolog 2, 6
MSI	microsatellite instability
NCI	National Cancer Institute
NEAA	non-essential amino acids
NHCME	normal human colon mucous epithelium
NMMU	Nelson Mandela Metropolitan University
NNMT	nicotinamide N-methyltransferase
p53	tumour protein 53
PB	phosphate buffer
PBS	phosphate buffer saline
PEG	polyethylene glycol
PMS2	postmeiotic segregation 2
PSME3	proteasome activator complex subunit-3
RES	reticuloendothelial system
SMAD	mothers against decapentaplegic homolog
SPR	surface plasmon resonance
Std dev	standard deviation
STEM	scanning transmission electron microscopy
TIMP-1	TIMP metallopeptidase inhibitor 1
TNM	tumour-node-metastasis
TSGs	tumour suppressor genes
UV/vis	ultra violet/visible
UV-IR	ultraviolet-infrared
ZP	zeta potential

LIST OF SYMBOLS

±	plus or minus
CM-1	per centimetre
g	gram
M	molar
mg	milligram
min	minutes
mL	millilitre
mM	milimolar
mol/l	moles per litre
nm	nanometer (10^{-9} meters)
^{o}C	degree celsius
w/v	weight per volume
v/v	volume per volume
µl	micro litre
µM	micro molar
%	percentage
m.V	milli- volts
kD	Kilodalton
mOsm	milliosmole

LIST OF FIGURES

Chapter 1

Figure 1.1: The anatomy of the large intestine 3

Figure 1.2: The adenoma-carcinoma sequence on colorectal cancer and the associated molecular mutations.....4

Figure 1. 3: The metabolism of DMH and AOM 9

Figure 1.4: A comparison between the sizes of nanoparticle and other molecules. 16

Figure 1.5: Schematic diagrams illustrating localized surface plasmon resonance.....18

Figure 1.6: Known cellular uptake pathways of nanoparticle 20

Figure 1.7: The intracellular uptake of nanoparticles through endosomal/lysosomal pathways. (ERC) Endocytic recycling compartment, (ER) Endoplasmic reticulum, (MTOC) Microtubule organizing centre, (MVB) Multivesicular bodies 21

Chapter 2

Figure 2.1: Overview of sample preparation process (A-E). (A) Grow and dose cells with AuNPs, (B) Cell processing (rinse, pellet, dehydrate, embedding), (C) Curing, (D) Trim and sectioning of sample, and (E) Imaging with HRTEM. 31

Figure 2.2: Schematic diagram of research design and electron microscopy evaluation 34

Figure 2.3: AOM/DSS method 1: The establishment of a CRC rat model. W1-14:Weeks 1-14, AOM–Azoxymethane injections (grey box), DSS- 2% dextran sodium sulphate administration (black box), dH_20- normal distilled water (White box), AuNP- AuNP injection (red box).....35

Figure 2.4: AOM/DSS method 2: The establishment of a CRC rat model. W1-14:Weeks 1-14, AOM-–Azoxymethane injections (grey box), DSS- 2% dextran sodium sulphate administration (black box), dH_20- distilled water (White box), AuNP- AuNP injection (red box).....36

Figure 2. 5: Rat necroscopy: (A) The tendon reflex is used to assess the level of consciousness of the rat, (B) Blood is removed from heart before necroscopy procedure, (C) The abdomen is cut exposing the abdominal viscera, and (D) The removal of the large intestine.....37

Chapter 3

Figure 3. 1: TEM Bright field (BF) images of (A) AuNPs-p.C, (B) AuNPs-p.L and (C) AuNPs-p.14. Black arrow indicates layer around AuNP. White arrow indicates lattice frindges. 42

Figure 3. 2: TEM (BF) micrographs of HT29 cell line treated with AuNPs-p.14 (A, B) Two arrows indicate the cell membrane; single arrow indicates the cell nucleus. 44

Figure 3. 3: TEM (BF) micrographs of HT29 cell line treated with AuNPs-p.C. (A, B) Two arrows indicate the cell membrane and single arrow indicates the cell nucleus.....45

Figure 3. 4: Average body weight (kg) at different time points between group 6 and group 1. AOM denotes the body weight taken on the day of AOM injection, C1, C2 and C3 denotes the weight taken at the end of cycle 1, 2 and 3. NP denotes the weight taken before AuNP injection. 50

Figure 3. 5: Examination of colon. (A) Image of colon showing no lesions, (B) Excision sites of rat colon lesions indicated by black arrows. 51

Figure 3. 6: Average body weight (kg) at different time points between group 6,group 2 and group 3. AOM-1, AOM-2 denotes the body weight taken on the day of AOM injection, C1, C2 and C3 denotes the weight taken at the end of cycle 1, 2 and 3. NP- denotes the weight taken before AuNP injection. 52

Figure 3. 7: TEM (BF) micrographs of colon tissue from inflamed regions of animals treated with AOM/DSS method 1, taken 24 hours after intravenous injection of AuNP-p.L. (Cf)- Collagen fibres, (N) Nuclei, (RER) Rough endoplasmic reticulum, (Mi) Mitochondria and (G) Golgi body. 54

Figure 3. 8: TEM (BF) micrographs of rectum tissue of AOM/DSS method 1, taken 24 hours after intravenous injection of AuNP-p.L. (Mv) Microvilli, (I) Interdigitations and a tight junction 55

Figure 3.9: TEM (BF) micrograph of pancreatic tissue of animals treated with AOM/DSS method 1, taken 24 hours after intravenous injection of AuNP-p.L. (ZG) Zymogen granules and (SER) Smooth endoplasmic reticulum. 56

Figure 3.10: TEM (BF) micrographs of kidney tissue of animals treated with AOM/DSS method 1, taken 24 hours after intravenous injection of AuNP-p.L. (N) Nucleus, (Mi) Mitochondria and (BM) Basal membrane. 57

Figure 3.11: TEM (BF) micrographs of healthy liver tissue from group 5, taken 24 hours after intravenous injection of AuNP-p.14. (RER) Rough endoplasmic reticulum, (Mi) Mitochondria and Tight junction (two black arrows). At higher magnification, electron dense particles indicated by single black arrow. 59

Figure 3.12: TEM (A) BF and (B) High angle annular dark field (HAADF) micrograph of heathy kidney from group 4, taken 24 hours after intravenous injection of AuNP-p.C. 59

LIST OF TABLES

Table 1: Molecular biomarkers for the detection of CRC 13
Table 2: Peptide-gold nanoparticle conjugates 28
Table 3: Glass knife preparation for ultrathin sectioning 39
Table 4: The characterisation of gold nanoparticles attached to peptide 42
Table 5: Parameters for optimal cell preservation. 46

CHAPTER ONE: LITERATURE REVIEW

1.1.General introduction

According to GLOBOCAN 2012, colorectal cancer (CRC) is the third most common and cause of cancer-related deaths worldwide (1.4 million, 9.7%), with 746,000 cases in men and 614,000 cases in woman. High incidence rates were found in Australia, Western, Southern and Northern Europe with a low incidence of colorectal cancer found in Africa (except South Africa), South America and Asia. In South Africa, colorectal cancer is the fourth most prevalent cancer (5.8%) and 6th leading cause of death (6.4%) (Ferlay *et al.*, 2013).

In Africa, 645,000 new cases of cancer and 456,000 deaths have been reported in 2012. This comprises 4.5% of the global cancer incidence and 5.6% of the global cancer mortality rate (Ferlay *et al.*, 2013). These rates are expected to double in 2030 due the aging, growth of the population and increase in the western lifestyle (Jemal *et al.*, 2012). Although the cancer burden in Africa appears to be very low, there is a possibility that this is not the true reflection for reasons that high-quality population-based cancer registries are not commonly available (Ferlay *et al.*, 2010). As an example, in South Africa, the last national cancer registry report made available has been in 2007 (CANSA., 2014). Colon carcinogenesis is a disease that requires years to develop, providing ample time for diagnosis and treatment. Unfortunately, it is common for majority of colonic tumours to go undetected until the cancer has progressed into a late stage where the tumour has metastasized (Kelly & Jones, 2003). In most parts of Africa, early detection and treatment services are limited. Conventional screening through colonoscopy is not only costly but not supported by the existing health care facilities whilst faecal occult blood tests (FOBTs) lack the needed sensitivity. Hence, there is a crucial need for the development of better diagnostic systems for colorectal cancer detection. The past decade has seen an explosion in our understanding of the cellular and molecular events in colorectal cancer. The identification of disease biomarkers and molecules (peptides, aptamers, antibodies, etc.) that can recognise these biomarkers specifically aims to improve early detection strategies through specific targeting. Together with nanotechnology, this creates a powerful diagnostics platform.

Previous studies have established the binding properties of three known phage display peptides (Shadidi & Sioud, 2003; Wang *et al.*, 2012; Wu *et al.*, 2000). Through fluorescence studies previously investigated by Mazyambe (2013) the interaction of these peptides towards colorectal cancer cell lines has been established. Much remains to be elucidated specifically on their cell uptake, localization and biodistribution in an *in vitro* and *in vivo* model. This is essential in gaining an understanding for future diagnostic or therapeutic based applications.

1.2.Background to colorectal cancer

Cancer is the term used for a disease in which abnormal cells in the human body start dividing and growing without control. CRC is a type of cancer that starts in the colon and rectum of the large intestine. It is a disease which has a long pre-malignant and asymptomatic development. Most CRCs starts with polyps occurring on the epithelial lining of the colon and rectum. These polyps may be benign (e.g. non-neoplastic), neoplastic polyps (e.g. adenomas, adenomatous) and cancers (Bardhan & Liu, 2013). CRC can be classified further into three observed populations; sporadic, inherited or familial (Johns & Houlston, 2001; Rustgi, 2007). In majority of cases, CRC occurs sporadically, whilst 3-4% of CRC cases are attributed to inherited mutations and 20-30% of patients reveal a family history of the disease (Johns & Houlston, 2001; Rustgi, 2007).

1.3.The structure and function of the large intestine

The large intestine forms a part of the digestive system and can be divided into three parts; the proximal (cecum, ascending colon and transverse colon), distal/left colon (descending colon, sigmoid colon) and the rectum (Fredericks, 2013). This system functions in processing food for energy and removes the solid waste as faecal matter (Fredericks, 2013; Keshav & Bailey, 2012). In addition to these functions, it is inhabited by a variety of commensal microbes aiding in colon physiology homeostasis. The colon consists of four basic layers - mucosa, submucosa, muscularis externa (longitudinal and circular) and the serosa, as seen in Figure 1.1. The mucous membrane forming the inner lining of the large intestine lack villi and contains numerous crypts composed of vast amounts of goblet cells, enterocytes and a few enteroendocrine cells. Covering this layer is the submucosa consisting of connective tissue embedded with large blood, nerve and lymphatic vessels. This extends to the muscularis externa an area consisting

of longitudinal and circular muscle. The outmost layer serosa consists of several layers of connective tissue.

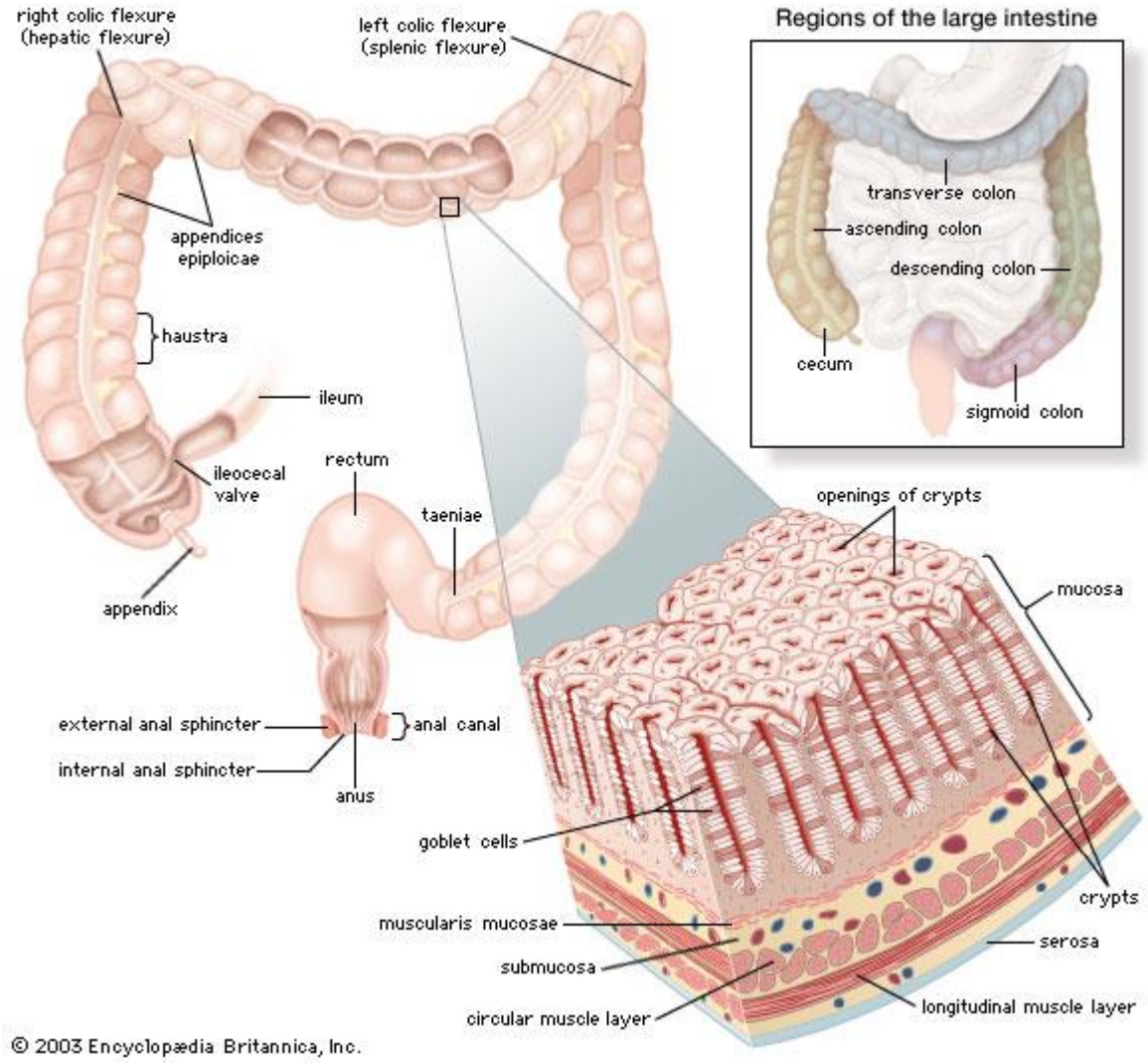

Figure 1.1: The anatomy of the large intestine (Encyclopaedia-Britannica.Inc, 2003).

1.4.Molecular bases of colorectal carcinogenesis

In 1990, Fearon and Vogelstein originally proposed the adenoma-carcinoma model describing colorectal carcinogenesis as a step-wise progression of genetic mutations (Fearon & Vogelstein, 1990). The altered genes include adenomatous polyposis coli (APC), tumour protein p53 (TP53 or p53), Kirstin ras (KRAS), chromosome 18 (i.e. this includes the deleted in colon cancer (DCC) and mothers against decapentaplege homolog (SMAD), as seen in Figure 1.2. These subsequent alterations perturb conserved signalling pathways which regulate cellular metabolism, differentiation, proliferation and survival. Ultimately transforming normal

epithelial cells to benign adenomas and malignant carcinomas (Chung, 2000; Fearon & Vogelstein, 1990).

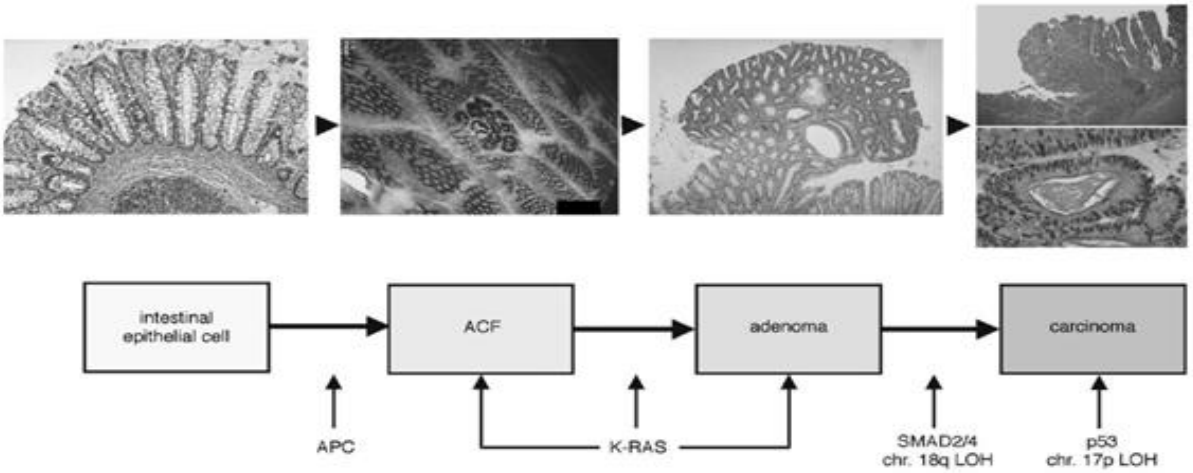

Figure 1.2: The adenoma-carcinoma sequence on colorectal cancer and the associated molecular mutations (Fodde, 2002).

1.4.1. APC/β-catenin and Wnt signalling pathway

Approximately 70-80% of sporadic adenomacarcinomas have somatic mutations of the APC gene. The APC gene is a tumour suppressor gene located on chromosome 5q21. It encodes a multifunctional protein with a molecular weight of ~310 kD, containing domains that interact with a scaffold protein Axin, β-catenin and serine-threonine glycogen synthase-3β (GSK-3β). (Fearon, 2011; Fodde, 2002). The APC gene product may regulate cell-cell adhesion, cell migration, apoptosis and cell regulation. However, its major role has been to participate in the formation of a multi-protein complex that's joins to β-catenin, causing its phosphorylation, subsequent ubiquitination and degradation of the β-catenin an essential component in the Wnt signalling pathway(Sameer, 2013). The loss of APC function disrupts β-catenin destruction resulting in the intracellular accumulation of active β-catenin in the cytoplasm. The β-catenin complexes with DNA-binding proteins resulting in its translocation to the nucleus where it begins to function as a transcriptional co-activator to various cell proliferation genes (Fearon, 2011; Sameer, 2013). Activating mutations in the β-catenin gene (CTNNB1) have also been observed in colorectal neoplasia (Morin *et al.*, 1997).

These APC mutations were first observed by familial adenomatous polyposis (FAP) an autosomal dominant disease (Leslie *et al.*, 2002).. FAP is caused by a germ-line mutation of APC gene leading to the development of hundreds of intestinal polyps at a relatively young age. If left untreated, 100% of individuals with the mutation will develop colorectal cancer

1.4.2. KRAS oncogene and the EGFR signalling pathway

KRAS gene is a proto-oncogene located on chromosome 12p12, encoding a ras protein with a molecular weight of 21kD (Fearon, 2011; Tan & Du, 2012). It is a guanosine-5'-triphosphate (GTP) binding protein with GTPase activity. When bound to GTP, the ras protein is active but becomes inactive when GTP is hydrolysed to guanosine diphosphate (GDP). Mutations of the KRAS gene occur in approximately 35-45% of CRCs. The ras protein is a downstream effector of the epidermal growth factor receptor (EGFR) that signals through the Braf protein and in turn, activates the MAPK pathway which is responsible for cellular proliferation and differentiation pathways.

1.4.3. p53 gene

The tumour suppressor p53 gene is located on the short (*p*) arm of chromosome 17. It encodes a 393 amino acid transcription factor responsible for maintaining genomic integrity by inducing cell cycle arrest or apoptosis when DNA is damaged. Mutations of p53 appear late in the adenoma-carcinoma sequence and are found in almost half of all colorectal cancer cases (Chung, 2000; Pritchard & Grady, 2010).

1.4.4. Chromosome 18q21 and TGF- β pathway

The allelic loss located on chromosome 18q has been identified in approximately 70% of colorectal tumours at more advanced stages of the tumourogenesis (Leslie *et al.*, 2002). It was initially thought that the tumour suppressor gene in this region was the "deleted in colorectal carcinoma" (DCC) gene, however the product of this gene was a cell surface receptor for neuronal protein netrin-1 (Keino-Masu *et al.*, 1996). Other tumour suppressor genes located on 18q region were also identified; these include the SMAD2 and SMAD4. The transcriptional products of both genes are involved in the transforming growth factor-β-(TGF-β) pathway (Chung, 2000; Fearon, 2011). In the TGF-β signalling pathway, signals through the TGFβ-cell

surface receptors leads to the phosphorylation of SMAD2 and SMAD3 proteins in mammalian cells. The SMAD2/3 protein complex enters the nucleus where they join to SMAD4. This protein complex then proceeds to regulate genes involved in the regulation of cell growth differentiation and apoptosis. Cable proteins, located on chromosome 18q11.2-12.1, have been marked as a relevent tumour suppressor gene. These proteins act as a linker protein facilitating the increase in tyrosine phosphorylation of cyclin-dependent kinases such as cdk2. The loss of cable expression has been shown to occur in 60-70% of sporadic colorectal cancers (Chung, 2000; Kirley *et al.*, 2005).

1.5.Colorectal cancer pathogenesis

Since the introduction of the adenoma-carcinoma model, knowledge of CRC development has advanced considerably. It is well known and reported that CRC arises as a result of the accumulation of genetic, epigenetic and DNA match repair gene mutations (Chung, 2000; Fearon & Vogelstein, 1990). The loss of genomic and epigenomic stability are the phenotypic features of colorectal carcinogenesis. Genomic instability has been observed by two pathways; these include the chromosomal instability (CIN) and microsatellite instability (MSI) pathway. Epigenetic instability in sporadic CRC have been demonstrated by the CpG island methylator phenotype (CIMP) pathway (Bardhan & Liu, 2013).

1.5.1. Chromosomal instability (CIN) pathway

Genomic instability has emerged as the fundamental process in colorectal carcinogenesis. The most common type of genomic instability is the CIN pathway also known as the adenoma-carcinoma sequence which accounts for approximately 60-70% of all CRC cases (Pancione *et al.*, 2012; Pino & Chung, 2010). The development of CIN tumours follows the predictable progression of mutations in oncogenes and tumour suppressor genes such as APC, TP53, KRAS, phosphoinositide 3-kinase (PI3KCA), SMAD4 and loss of heterozygosity (LOH) as seen in Figure 1.2 (Fodde, 2002). CIN tumours are characterized as having an imbalance of chromosome numbers (aneuploidy) and loss of heterozygosity. These tumours are predominantly found in the right (distal) colon (Cardoso *et al.*, 2007; Rosner & Strul, 2014).

1.5.2. Microsatellite instability (MSI) pathway

The inactivation of the mismatch repair mechanism (MMR) may result in genomic and epigenomic instability. The MMR mechanism corrects errors that spontaneously occur as a result of DNA damage, oxidative stress or following DNA replication errors (Armaghany *et al.*, 2012). Microsatellites are short repetitive DNA nucleotide sequences prone to frame shift mutations and base-pair substitutions during replication. If the MMR system is deficient within the cell, this creates microsatellite instability. Unlike the CIN pathway, this pathway is relatively well understood, near-diploid and are predominantly found in the left (proximal) colon (Cardoso *et al.*, 2007). This pathway accounts for 15% of all CRC, 5% being Lynch syndrome or hereditary non-polyposis colorectal cancer syndrome (HNPCC) (Pritchard & Grady, 2010). Individuals with Lynch syndrome present germline mutations in the MMR genes. Ninety percent of all Lynch syndrome cases occur from mutations in one or two major genes, MutL homolog 2 (MSH2) and MutS homolog 1 (MLH1) (Goel & Boland, 2010). The remaining 10% of cases arise from mutations in the other MMR genes; MutS homolog 6 (MSH6), postmeiotic segregation 2 (PMS2) and MutL homolog 3 (MLH3).

1.5.3. CpG island methylator phenotype (CIMP) pathway

The CpG (cytosine preceding guanosine) island methylator phenotype (CIMP) pathway is the third pathway to the development of sporadic colorectal cancer and accounts for approximately 12-25% of CRCs (Pitule *et al.*, 2013). The CIMP pathway creates epigenomic instability characterized both by hypermethylation of promoters that contain CpG islands and global DNA hypomethylation (Pancione *et al.*, 2012; Pritchard & Grady, 2010). More than 50% of human genes have been shown to be regulated by promoters containing CpG islands. However, in CRC, CpG islands have been shown to be hypermethylated resulting in the silencing of tumour suppressor genes. In contrast to CIN tumours, CIMP tumours show less aneuploidy and frequently develop within the left (proximal) colon (Venkatachalam *et al.*, 2010). CIMP tumours have been associated with BRAF and KRAS mutations through the MAPK pathway however CIMP tumours arise from serrated rather than adenomatous polyps.

1.6.Animal model for colorectal carcinogenesis

There exist several experimental models for the investigation of colon carcinogenesis; these can be divided into colorectal cancer cell lines or animal models (Robertis *et al.*, 2011). Animal models are important tools, providing us with a larger insight into the pathogenesis of CRC, but also advancing our understanding of therapeutic and diagnostic strategies (Ravnik-Glavač *et al.*, 2000; Robertis *et al.*, 2011). The ultimate goal of modelling CRC in animal models is to recapitulate the disease as seen in humans. Johnson and Fleet (2013) describe three characteristics essential to maintaining this goal. First, the cancer should only be situated in the large intestine where the disease is predominantly seen in humans. Secondly, the colonic lesions should represent the histological and molecular features of human CRC and thirdly, the model should capture the complex cellular interactions that are relevant to human colon cancer. The CRC animal models can broadly be divided into spontaneous intestinal cancers, chemically/environmentally-induced or genetically modified rodents (Johnson & Fleet, 2013). Carcinogen–induced colorectal cancer has shown to be superior to all animal models as CRC pathogenesis occurs sporadically and undergo similar molecular alterations found in human colorectal carcinogenesis (Robertis *et al.*, 2011; Rosenberg *et al.*, 2009). These models are highly reproducible and can be readily tested on animals with different genetic backgrounds.

1.6.1. Dimethylhydrazine and Azoxymethane

Dimethylhydrazine (DMH) and its metabolite, Azoxymethane (AOM), are the two most commonly used carcinogens to induce CRC in rodents. This is a less expensive, more potent and convenient model to use with majority of tumours developing within the distal colon, with a low frequency within the small intestine (Rosenberg *et al.*, 2009). DMH is metabolically activated to DNA-reactive products by multiple xenobiotic-metabolizing enzymes (Druckrey, 1970; Fiala, 1977; Rosenberg *et al.*, 2009). This produces intermediates, AOM and methylazoxymethanol (MAM) which can be transported to the colon or enter the enterocytes from blood circulation, as seen in Figure 1.3. MAM is unstable, and readily yields the mutagen methyldiazonium ion either spontaneously or through alcohol dehydrogenases. This product is capable of altering the information of DNA through methylation but also modifying histones and DNA-binding proteins (Fiala, 1977; Perše & Cerar, 2005). The majority of DMH/AOM tumours harbour β-catenin and K-RAS mutations, with elevated levels of COX-2 and inducible

nitric oxide synthase (iNOS-2) similar to the genetic and molecular alterations in sporadic human colorectal carcinogenesis (Takahashi *et al.*, 2000; Yoshimi *et al.*, 2009).

In 1973 DMH-induced colon cancer was seen as an effective experimental model for sporadic CRC. DMH was administrated with weekly subcutaneous injections for 7 months. This resulted in rats developing intestinal tumours similar to human colorectal adenomas (Martin *et al.*, 1973). Later studies done by Deschner and Long (1977) have shown the reduction of subcutaneous injections to 6 injections over a period of 7 months resulted in neoplasms found in 83% of the mice (Deschner & Long, 1977). An increasing number of studies, however, switched to the AOM as it offers several advantages over DMH. This includes enhanced potency, greater stability in a dosing solution, and higher reproducibility (Rosenberg *et al.*, 2009). When using single or multiple injections of DMH/AOM, colon tumour development have shown a low tumour incidence and long latency period of 7 to 8 months (Neufert *et al.*, 2007; Tanaka *et al.*, 2003). However, with the subsequent treatment using dextran sulphate sodium (DSS), tumour development could take as little as 7-10 weeks (Thaker *et al.*, 2012).

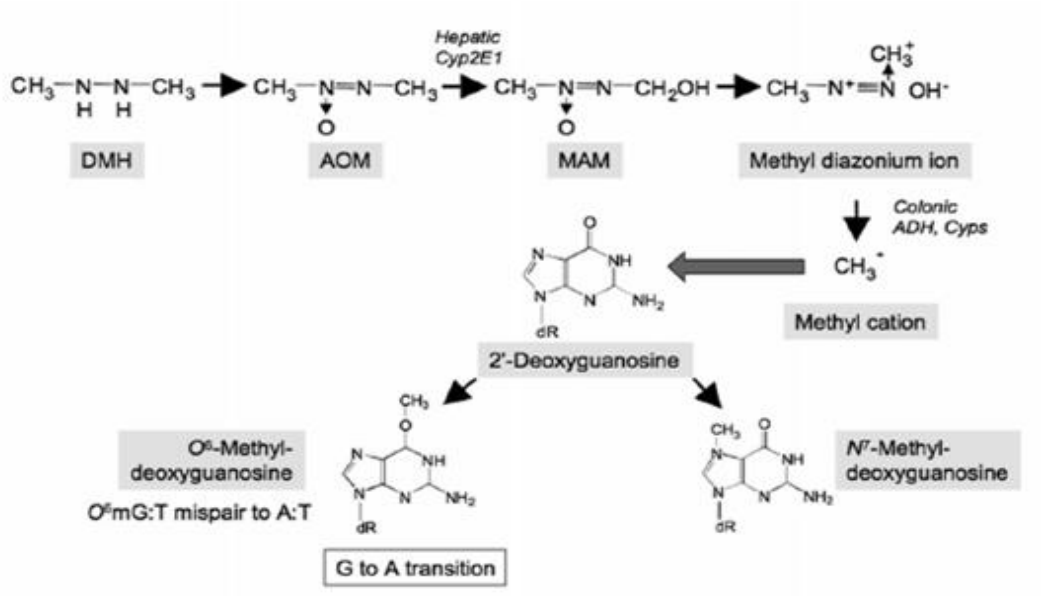

Figure 1. 3: The metabolism of DMH and AOM (Rosenberg *et al.*, 2009).

1.6.2. Dextran sulphate sodium

Dextran sulphate sodium (DSS) is a non-genotoxic sulphated polysaccharide used to induce colitis (inflammation to the epithelial lining of the colon) when administrated through diet or drinking water (Suzuki *et al.*, 2005). Through DSS administration, colonic inflammation could resemble that of inflammatory bowel disease or ulcerative colitis. With a long term administration, colonic malignancies are induced which resemble the adenoma-carcinoma sequence as discussed in section 1.4. According to Perše and Cerar (2012) the tumour promoting effects of DSS is dependent on various factors which include the administration dose, duration, molecular weight, the batch, manufacturer and genetic susceptibility of rodent (strain, substrain and gender) (Perše & Cerar, 2012). It is also suspected that microbial factors could play a role. According to Suzuki *et al.* (2005), the tumour promoting effect of DSS (molecular weight of 40 kDa) is strongly related to the administration dose. The literature suggests that the exposure to DSS in drinking water at a dose of 1% to 2% DSS for 1 week after a single injection of AOM (10 mg/kg body weight) could produce multiple colonic neoplasms within 20 weeks compared with mice treated with AOM and given lower doses (0.5, 0.25 and 0.1% w/v DSS). This suggests that at a higher DSS dose, severe inflammation contributes to the tumour promoting effects in rodents. No such study has looked at the dose-dependent promoting effects of different DSS molecular weights.

1.6.3. AOM/DSS- induced carcinogenesis model

Taking into consideration the long term experimental period needed to induce colonic tumours using AOM (tumour-inducing agent) or DSS (tumour-promoting) alone, the AOM/DSS method was developed to dramatically increase tumour development to as little as a few weeks (Tanaka *et al.*, 2003). The AOM/DSS treated rodent model is also applicable when the study is focused on tumour development as a result from ulcerative colitis or crohns disease. Historically, colon carcinogenesis studies have been carried out in rats. However, murine models holds an advantage due to availability of extensive genetic information on individual mouse lines (Robertis *et al.*, 2011; Thaker *et al.*, 2012). The AOM/DSS rodent model has been proven to be highly valuable for its ability to produce tumours mirroring the various pathological aspects of human CRC and for investigating novel diagnostic, prognostic or chemotherapeutic agents against CRC (Robertis *et al.*, 2011).

1.7. Colorectal cancer screening tools

Research has indicated that patients presenting stage I or II of CRC disease have a 5 year survival rate of 93.2% and 82.5% respectfully, when treated with surgery or when surgary is combined with chemotherapy (Bianchi *et al.*, 2011). CRC survival rates are drastically reduced at later stages of the disease with patients having a 59.5% and an 8.1% survival rate of stage III and IV disease (O'Connell *et al.*, 2004). Although survival is strongly linked to the stage of CRC diagnosis (Coetzee, 2013; García-Bilbao *et al.*, 2012). However; early diagnosis of CRC becomes difficult as CRC symptoms only appear are common in advanced stages where lesions are often higher grade and incurable (Kanthan *et al.*, 2011). Randomized trials suggest that early detection of cancer through screening has proven to reduce CRC mortality (Hardcastle *et al.*, 1996; Kronborg *et al.*, 1996; Scholefield *et al.*, 2002). However, there are several pitfalls to the screening tools available. The current CRC screening tools in practise are endoscopic and the biomarker screening.

1.7.1. Endoscopic screening

Colonoscopy is currently considered the "gold standard" (Kanthan *et al.*, 2011). It is a tool used to visualize the mucosa wall of the colon, remove pre-malignant lesions, malignant tumours or adenomas up to 100% (Coetzee, 2013). Despite its high reliability this technique has several limitations. Colonoscopy is an invasive tool requiring sedation and full bowel preparation (Baxter & Rabeneck, 2008; Rex *et al.*, 1997). It can be costly and requires experienced physicians. Consequently, it lacks patient compliance. Colonoscopy examination also presents a miss rate of adenomas by 24% as visualization of the full length of the colon cannot be seen (Rex *et al.*, 1997). This miss rate also increases up to 27% for flat and depressed adenomas smaller than 5 mm. Except for one case controlled study showing a reduction of 67% in mortality only for left-sided colorectal cancer (Baxter & Rabeneck, 2008), there are currently no other randomized control trials available to draw conclusions as to whether this technique reduces CRC mortality.

Flexible sigmoidoscopy is a tool less invasive than colonoscopy. It is based on the visualization of the mucosa of the left colon with tissue biopsy (Coetzee, 2013). This technique does not require the use of trained physicians which consequently lowers the cost of examination. Randomized controlled trials have shown that screening programmes using flexible

sigmoidoscopy reduced mortality by detecting early CRC lesions and advanced adenomas (Baxter *et al.*, 2009; Kronborg *et al.*, 1996; Littlejohn *et al.*, 2012). However, this detection tool is limited as adenomas proximal to the colon may be missed.

1.7.2. Biomarker screening

Biomarkers are indicators of a biological state. These biomarkers can be used as a diagnostic tool or to study the normal, pathogenic or pharmacological processes (Tanaka *et al.*, 2010). At present, the faecal occult blood test (FOBT) is the widely used fecal marker for CRC screening (Tanaka *et al.*, 2010). FOBT is based on rectal bleeding associated with CRC, detecting haemoglobin enzymatically or immunologically in the stool(Kanthan *et al.*, 2011). The advantage of this method is its relative low cost, tests simplicity, safety, and non-invasiveness. Through randomized controlled trials conducted by Littlejohn *et al.* (2012), FOBT has shown to reduce CRC mortality by 21%. However, the FOBT is limited as the sensitivity for the detection of pre-cancerous lessions (~ 30%) and CRCs (40-85%) are low (Kanthan *et al.*, 2011; Tanaka *et al.*, 2010). This detection tool may falsely react to heme in red meat or detect bleeding from the stomach or small bowel, frequently reporting false-positive and false-negative results.

The increase in genomics and proteomics contributed to our molecular understanding of CRC (García-Bilbao *et al.* (2012).This has helped identify genes and/or proteins that would aid in the early detection of CRC. To our knowledge such markers are currently being used or have yet to be clinically validated. See Table 1. (Tanaka *et al.*, 2010).

Serum biomarkers such as CEA and CA 19-9 are in clinical use for disease state evaluation, but are often unemployed for screening purposes due to lack in sensitivity and specificity where they show an overlap with other disease such as hepatisis, inflammatory bowel disease or pancreatisis. Other serum based markers are have insuffecient evidence for routine use whilst genetic markers are not wideley used in clinical settings. Other biomarkers remain promising but still need to be clinically validated (García-Bilbao *et al.*, 2012; Tanaka *et al.*, 2010).

Table 1: Molecular biomarkers for the detection of CRC (Tanaka *et al.*, 2010).

Colorectal Cancer Biomarkers	**Subject**	**Type**	**Status**
Faecal haemoglobin	Stool	Protein	IU
K-ras	Stool	DNA	CV
APC	Stool	DNA	CV
L-DNA	Stool	DNA	CV
p53	Stool	DNA	CV
CEA	Serum	Protein	IU
CA19.9	Serum	Carbohydrate	IU
TIMP-1	Serum	Protein	CV
Spondin-2, DcR3, Trail-R2, Reg IV, MIC 1	Serum	Protein	PD
PSME3	Serum	Protein	PD
NNMT	Serum	Protein	PD
CRMP-2	Serum	Protein	PD
SELDI (apolipoprotein C1, C3a-desArg, alpha1-antitrypsin, transferrin)	Serum	Protein	PD
HNP 1-3	Serum	Protein	PD
MIF	Serum	Protein	PD
M-CSF	Serum	Protein	PD
M2-PK	Serum	Protein	PD
Prolactin	Serum	Protein	PD
Septin 9	Plasma	DNA	PD
Five-gene panel (CDA, BANK1, BCNP1, MS4A1, MGC20553)	WBC	DNA	PD
CCSA-2, -3 -4	Serum	Protein	PD
MMP-9, -7	Serum	Protein	PD
Laminin	Serum	Protein	PD

IU: in use, CV: clinical validation, PD: preclinical development

An ideal screening technique requires a combination of early-stage cancer detection, high sensitivity and specificity, affordability, non-invasiveness, safety, wide scale applicability and a high patient compliance (Coetzee, 2013; Kanthan *et al.*, 2011). These current screening tools (colonoscopy, flexible sigmoidoscopy and FOBT) do not meet this standard (Tanaka *et al.*,

2010). Consequently there is a need for the development of novel non-invasive biomarkers capable of enhancing the early detection of the disease.

1.8.Colorectal cancer targeting peptides

1.8.1. Why peptides?

Biomarkers can exist as antibodies, peptides, nucleic acid or others such as carbohydrates or vitamins (Ladner *et al.*, 2004; Yu *et al.*, 2012). Antibodies are the popular and conventional candidates for tumour recognition and drug delivery. They are assumed to have high specificity and affinity, large-reproducibility, acceptable toxicity, predictability, a favourable cost and low antigenicity (Ladner *et al.*, 2004; Patri *et al.*, 2004; Sapra & Allen, 2002). However, there are several limitations which include; their large size which restricts passage through the endothelial cell membrane capillaries resulting in poor delivery to tumours and their difficulty in conjugating the antibodies to delivery carriers e.g. nanoparticles (Yu *et al.*, 2012).

Serum biomarkers such as CEA and CA 19-9 (Table 1) are in clinical use for disease state evaluation, but are often unemployed for screening purposes due to lack in sensitivity and specificity where they show an overlap with other disease such as hepatitis, inflammatory bowel disease or pancreatitis. Other serum based markers have insufficient evidence for routine use whilst genetic markers are not widely used in clinical settings. Other biomarkers remain promising but still need to be clinically validated (García-Bilbao *et al.*, 2012; Tanaka *et al.*, 2010).

Peptides on the other hand have been receiving greater attention due to their small size, better tumour penetration, selective binding and their ability to evade the immune system unlike antibodies.

1.8.2. The identification of cancer specific peptides

Combinatorial peptide library technology have made it possible to identify peptides possessing binding specificity for tumour receptors, enzymes or antibodies (Shadidi & Sioud, 2003).Numerous specific peptides have been identified specifically p.C, p.14 and p.L which will be discussed in detail.

Due to a confidential agreement, the sequences of the peptides are not mentioned here.

p.C was discovered by Wu *et al.* (2000) using random phage display and was raised against prostate specific antigen. This study showed that this particular peptide bound specifically towards prostate cancer cells. However; Mazyambe (2013) has demonstrated the specific binding of this peptide towards cancer cell lines not of prostate cancer origin. In Mazyambe (2013) study, p.C has demonstrated to bind to Caco-2 and HT29 (colorectal cancer cell lines) with high specificity compared to other cell lines. This study reported that p.C peptide was unable to bind to a non-cancerous cell line and can thus be used to differentiate between cancerous and non-cancerous tissue (Mazyambe, 2013)

p. L was discovered by Shadidi and Sioud (2003) using random phage display. The study showed that p.L was capable of preferential binding and internalization into breast cancer cell lines. However; this peptide was re-tested and showed strong binding towards glioma cell line BT4C (Shadidi & Sioud, 2003). Another study has shown that the p.L peptide has a binding specificity towards cancer cells that over express the ErbB-2 growth factor receptor (Wang *et al.*, 2007). Mazyambe (2013) has demonstrated the specific binding of this peptide towards HT29 colorectal cancer cells compared to Caco-2, Hela, HepG2 and Kmst-6 cell lines.

Wang *et al.* (2012) discovered five colorectal binding peptides from a random phage display library. p.14 was specifically analysed using immunofluorescence. Results indicated that this peptide was able to bind more favourable to LoVo cells than to normal human colon mucous epithelium (NHCME) cells. The study by Wang *et al.* (2012) recommended that a colorectal animal model should be used to evaluate the binding specificity of this peptide and to the best of our knowledge such a study not yet done.

1.9.Nanotechnology based- delivery systems

Nanotechnology is defined as the controlled manipulation of devices at one billionth of a metre (10^{-9} M). The concept of nanotechnology was first introduced by Richard Feyman. In his letter titled “There is plenty of room at the bottom”, Feyman wrote that properties of material at an atomic scale differ considerably to material at their bulk scale, as they are governed by the law of quantum mechanics (Feynman, 1960). These unique physicochemical properties include an increased surface area, increased chemical reactivity, novel optical, magnetic and thermal properties (Jain *et al.*, 2007; Sahoo *et al.*, 2007). A large focus has been placed on cancer

nanotechnology specifically on the development of novel diagnostic, therapeutic and monitoring tools. Nanoparticles are similar in size to that of biomolecules such as proteins (1-200nm), DNA (~2 nm) and the cell membrane (6-10 nm), see figure 1.4 (Patra *et al.*, 2010). This makes nanoparticles capable of overcoming biological barriers such capillary vessels and preferentially accumulating in tumours (Cai *et al.*, 2008; Wang & Thanou, 2010).

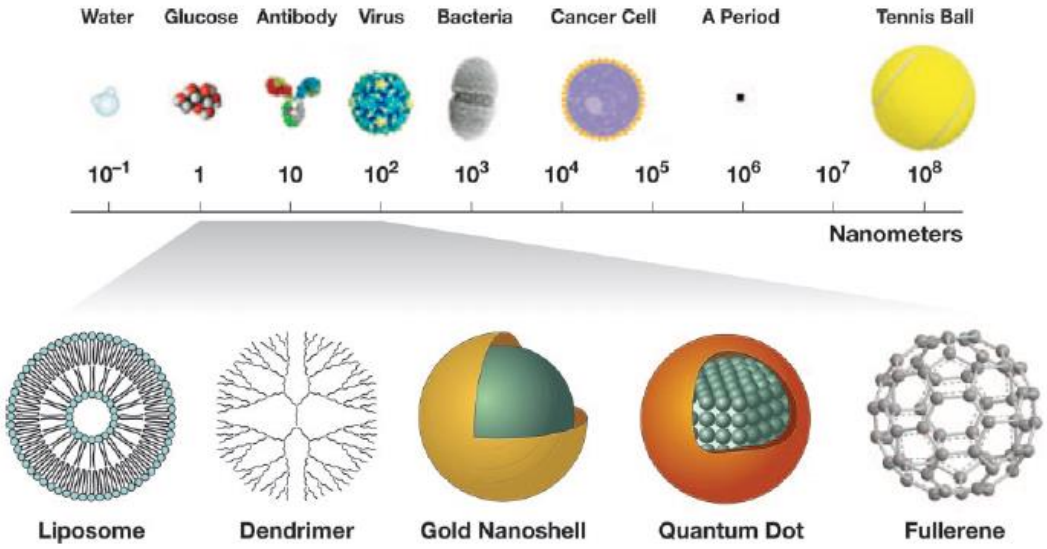

Figure 1.4: A comparison between the sizes of nanoparticle and other molecules (McNeil, 2005).

1.9.1. Gold nanoparticles

The use of colloidal gold for medicinal and decorative purposes is dating back to 2500 BC. Historically, alchemists would make Aurum portable (drinking gold) for the treatment of fevers, syphilis or epilepsy. In 1927, colloidal gold was shown to possess healing properties and was used for the treatment of rheumatoid arthritis (Antonovych, 1981; Higby, 1982; Thakor *et al.*, 2011). Today the use of gold nanoparticles (AuNPs) has expanded in biomedical research. Due to their unique properties they are used in diagnostic, therapeutic or theranostic applications (Patra *et al.*, 2010).

Gold nanoparticles can easily be synthesized in a variety of shapes (spheres, rods, tubes, wires, cubic, hexagonal, triangular) and sizes (5-200 nm) due to controlled changes in chemical

reaction parameters (Patra *et al.*, 2010). The most common method of gold nanoparticle synthesis is through chemical reduction of gold (III). This is an economically cheap, safe and reliable method, first reported Turkevich *et al.* (1951) and later improved by Frens (1973) and Kimling *et al.* (2006). In this method gold nanospheres are created by the addition of trisodiumcitrate to a heated aqueous solution of tetrachloroauric acid. This results in the nucleation of gold ions which are then stabilized by the remaining citrate molecules forming a negative AuNP surface charge (Zhao *et al.*, 2013). The negative surface charge increases reactivity of AuNPs, allowing for surface functionalization of biomolecules (peptides, DNA, antibodies, etc.).

1.9.1.1.Gold nanoparticle optical properties

Gold nanoparticles have attracted considerable attention due to their unique optical properties. Gold in bulk is seen as a familiar yellow colour, however with the reduction in size and dimensionality of gold, a drastic change occurs in the electronic properties due to the reduction in spatial length of electron motion (El-Brolossy *et al.*, 2008). When incident light interacts with the free d electron on the surface of Au core, this creates a collective coherent oscillation of electrons across the surface of the nanoparticles known as surface plasmon resonance (SPR), as seen in Figure 1.5 (Willets & Van Duyne, 2007). The surface plasmon oscillation of the metal electrons results in a strong enhancement of absorption and scattering of light (Sokolov *et al.*, 2003).

Gold nanoparticles can be seen as a contrast agent in cellular and biological imaging applications. Contrast agents greatly increase the sensitivity of an imaging technique, this allows us to visualize previously undetected abnormalities in cells or tissue of interest. The current contrast agents include flourometric, chemiluminescent or colorimetric techniques. These probes often suffer from weak optical signals and photobleaching. Gold nanoparticles have become an alternative consideration due to their SPR, non-photobleaching and non-cytotoxicity properties (Jain *et al.*, 2007).

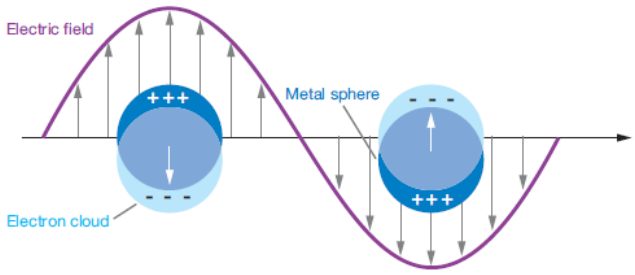

Figure 1.5: Schematic diagrams illustrating localized surface plasmon resonance (Willets & Van Duyne, 2007).

Taking advantage of gold nanoparticles absorption properties, gold nanoparticles have been used as a contrast agent in photoacoustic imaging (Mallidi *et al.*, 2009). Whilst, El-Sayed *et al.* (2006) has demonstrated the difference between cancerous and non-cancerous cells through dark-field microscopy and absorption spectroscopy. Luo *et al.* (2010) has demonstrated the ability to create a new multiplexing detection scheme using differential interference contrast microscopy. Similarly, Sokolov *et al.* (2003) have has exploited the strong light scattering of gold nanoparticles for real-time optical imaging of pre-cancer and cancers by using confocal reflectance microscopy. In addition to this, gold nanoparticles have a high X-ray attenuation factor. They have been widely used for labelling and staining of biological specimens for electron microscopy (D'amico & Skarmoutsou, 2008; Liou *et al.*, 1996; Mayhew, 2009) which will be discussed later in detail.

1.9.1.2.Gold Nanoparticle *in vivo* diagnostic applications

The unique properties and the use of gold for the treatment of human disease (e.g. rheumatoid arthritis) have made gold nanoparticle an attractive agent for *in vivo* diagnostic applications. As discussed above, gold nanoparticles have been used as contrast agents in *in vitro* based applications based on their ability to scatter visible light. One of the greatest limitations in *in vivo* diagnostics is the non-invasive early detection of cancer. Standard clinical imaging technologies such as MRI, CT, X-ray and PET are becoming routinely used in hospitals (Gu, 2011; Popovtzer *et al.*, 2008). These tools provide us with anatomical information of the body through the use of contrast agents which assist in providing greater sensitivity. These tools are structural imaging modalities as opposed to molecular imaging modalities as they identify tumour location, size and spread. They are not efficient in distinguishing between benign and

cancerous tumours or the detection of tumours less than 0.5 cm. As demonstrated by Reuveni *et al.* (2011), gold nanoparticles have a high X-ray attenuation coefficient in comparison to the conventional contrast agents such as iodine. By conjugating a targeting molecule (antibody, peptide, aptamers, etc.) to gold nanoparticles, gold nanoparticles demonstrate specific targeting towards cancer receptors in tumours through an active targeting mechanism as opposed to the passive targeting which deals with the enhanced permeability and retention effect (EPR) (Arvizo *et al.*, 2011). In this way, active tumour identification and the strong attenuation of gold provide an increased tumour specificity and sensitivity. This will provide practitioners a non-invasive CT imaging tool which can facilitate the early detection of cancer based on specific biomarkers rather than on anatomical structures (Reuveni *et al.*, 2011).

1.10. The uptake and distribution of gold nanoparticles

In order for nanoparticles to be taken into cells and their subcellular structures, nanoparticles must be able to cross the plasma membrane. Polar or charged biomolecules such as amino acids, glucose, proteins etc. require active transport via endocytosis pathways or specific transporters. Nanoparticles exist in the 1-100 nm size range, similar to the size of biomolecules (Kettiger *et al.*, 2013). Experimental studies have revealed that nanoparticles are taken up in a similar way than biomolecules, depending on their size (Chithrani *et al.*, 2006; Mironava *et al.*, 2010; Sonavane *et al.*, 2008), shape (Chithrani *et al.*, 2006), chemical composition (Kulkarni & Feng, 2013; Raschke *et al.*, 2004) and surface functionality (Chanda *et al.*, 2010; Li *et al.*, 2009; Lund *et al.*, 2011; Shi *et al.*, 2012). An additional factor is protein absorption onto the surface of the nanoparticle forming a protein corona and this changes the physicochemical properties of the nanoparticles which could affect the rate of cell uptake (Shi *et al.*, 2012). Chithrani *et al.* (2006) has investigated the intracellular uptake of 14, 30, 50, 74, and 100 nm spherical and rod shaped gold nanoparticles. Their findings from this study suggested that spherical nanoparticles have a higher probability of entering the cells in comparison to rod nanoparticles. Results have indicated that nanoparticles with a diameter of 50 nm are most efficiently internalized by cells than nanoparticles between 30 -50 nm which are subsequently taken up by receptor- mediated endocytosis (Chithrani *et al.*, 2006). Their results also suggest that non-specific absorption of serum proteins could play a role in mediating the intracellular mechanism and uptake of the nanoparticles. Unbound citrate-stabilized gold nanoparticles have

shown greater uptake compared against protein absorbed nanoparticles as they compete for receptor sites (Chithrani *et al.*, 2006), as seen in Figure 1.6.

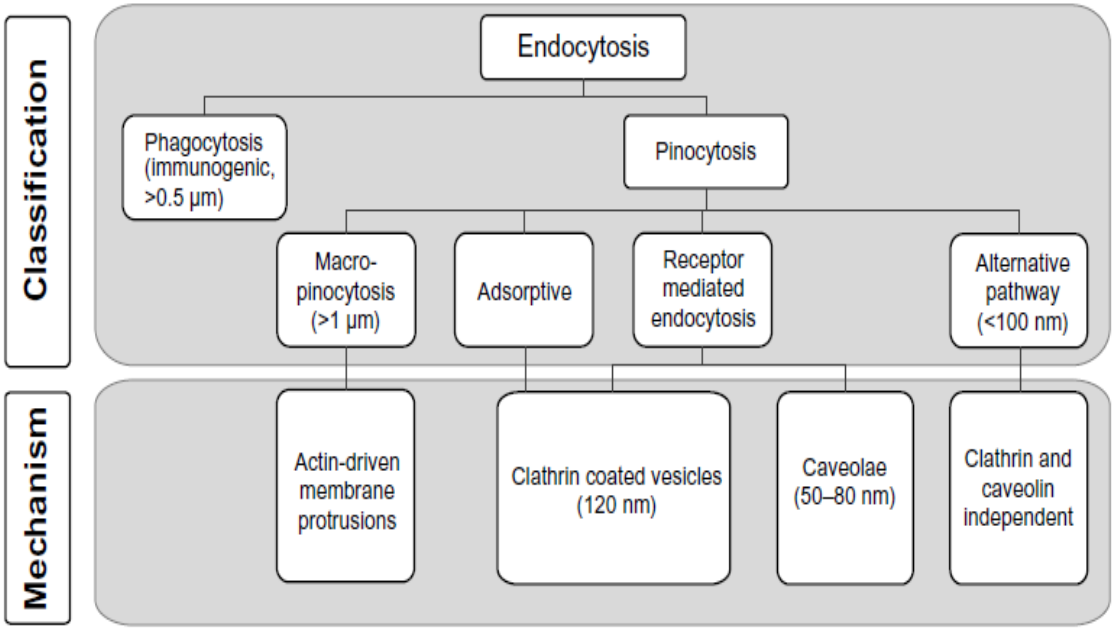

Figure 1.6: Known cellular uptake pathways of nanoparticle (Kettiger *et al.*, 2013).

The endocytic pathways can be classified into phagocytosis and pinocytosis. Phagocytosis is a process whereby cells of the immune system such as macrophages, monocytes and neutrophils internalize nanoparticles larger than 500 nm (Kettiger *et al.*, 2013). Small molecules ranging from few to several nanometres are generally taken up in almost all cells by pinocytosis. Pinocytosis can be further classified into (i) macropinocytosis (ii) absorptive pinocytosis and mainly (iii) receptor-mediated endocytosis. Receptor mediated endocytosis occurs predominantly via clathrin-mediated endocytosis (CME) or caveolae-mediated endocytosis (CvME), as seen in Figure 1.6 (Chithrani *et al.*, 2006; Kettiger *et al.*, 2013; Treuel *et al.*, 2013).

Endocytosis transports nanoparticles into cells within vesicles. Depending on their mode of internalization, nanoparticles can be subjected to endosomal/lysosomal pathways, as seen in Figure 1.7. Intracellular vesicles can either transport their content to endosomes or exocytose the content back to the cell surface. Some nanoparticles are able to escape the endosomes and access the cytoplasmic and nuclear targets (Chou *et al.*, 2011; Kettiger *et al.*, 2013).

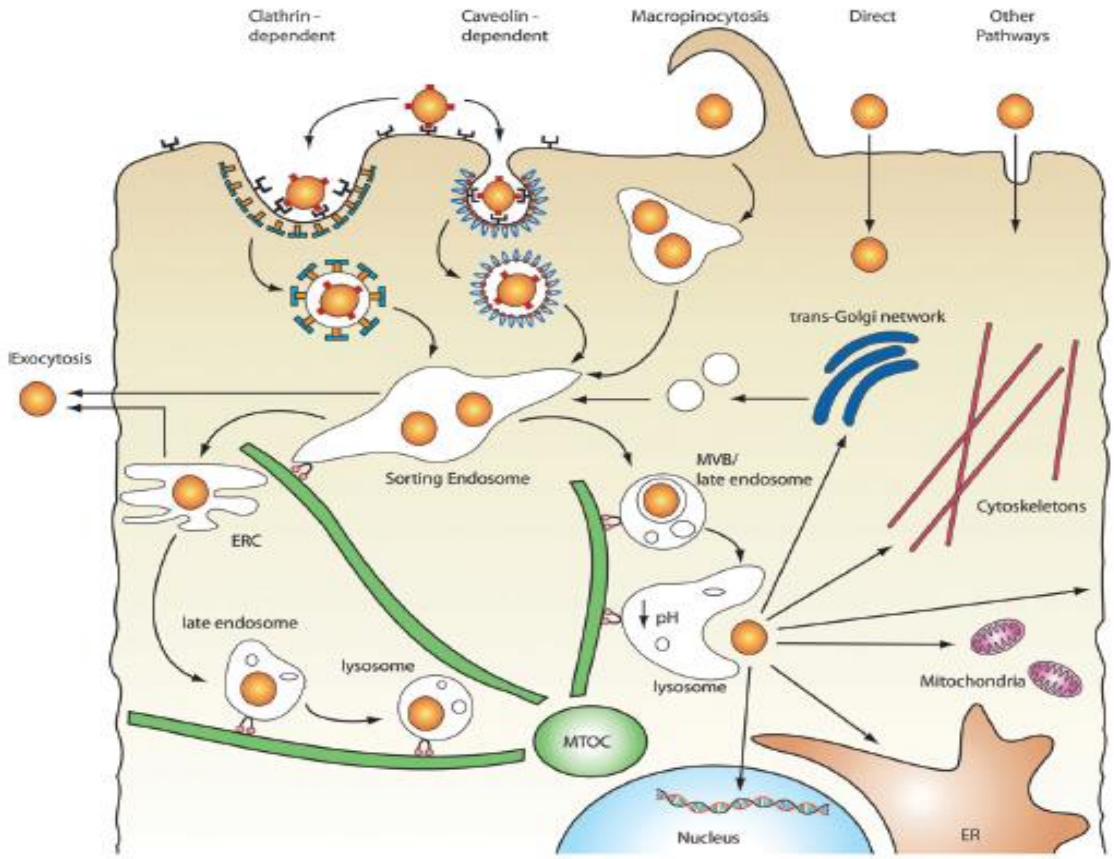

Figure 1.7: The intracellular uptake of nanoparticles through endosomal/lysosomal pathways. (ERC) Endocytic recycling compartment, (ER) Endoplasmic reticulum, (MTOC) Microtubule organizing centre, (MVB) Multivesicular bodies (Chou *et al.*, 2011).

Nanoparticle biodistribution studies is the method for understanding the intracellular trafficking and fate of nanoparticles in an *in vivo* system (Tiwari *et al.*, 2011). Although it is known that nanoparticle distribution is influenced by the size (Cho *et al.*, 2009; Sonavane *et al.*, 2008; Zhang *et al.*, 2011), shape, medium composition and surface chemistry of nanoparticles, the *in vivo* system reveals that circulation, distribution, degradation and excretion need to be taken into consideration. These complex relationships are still only partially understood (Morais *et al.*, 2012).

The most widely used route for nanoparticle administration is the intravenous route (IV). This route has direct access to the blood circulation allowing for rapid distribution throughout the body (Hirn *et al.*, 2011). One of the first concerns of nanoparticle injection is their state of dispersion within solution as agglomerates may cause an embolism. When nanoparticles reach the systemic circulatory system, they are encounter blood constituents such as plasma proteins (e.g. albumin, opsonins) prior to their encounter with the plasma membrane of cells (Morais *et*

al., 2012). A protein corona forms on the surface of the nanoparticle changing the surface properties of the nanomaterial.

In vivo biodistribution studies of AuNP have been increasing over the past few years focusing mainly on citrate-coated AuNP intravenously injected into rats (Balasubramanian *et al.*, 2010; Hirn *et al.*, 2011; Lipka *et al.*, 2010) or mice (Cho *et al.*, 2010; Sonavane *et al.*, 2008). The findings of these studies suggest that the distribution of AuNPs, taken 24 hours after intravenous injection were proved to be dependent on the size of the injected nanoparticle. According to Jong et al (2008), the smallest particle, 10 nm had a widespread distribution with a higher concentration found within the liver followed by the blood, spleen, kidney and lungs. 10, 100, 250 nm AuNps were mostly found in the liver, spleen and blood (Balasubramanian *et al.*, 2010; De Jong *et al.*, 2008). A positively charged surface has also shown to affect the biodistribution of AuNP resulting in their accumulation within the kidneys whilst non-charged or negatively charged particles showed a high accumulation within the liver (Balogh *et al.*, 2007).

One of the obstacles that nanoparticles face is the reticuloendothelial system (RES). The reticuloendothelial system (RES) consists of fixed macrophage cells within organs such as liver, spleen, lymph nodes, kidney, lung and bone marrow as well as circulating macrophages and monocytes. The purpose of this system is to remove any foreign material in the body (Gupta & Kompella, 2006). Small size nanoparticles (<20 nm) have been shown to avoid the RES as they attract fewer opsonins resulting in longer distribution within the capillaries and tissues (Papasani *et al.*, 2012). Another way to overcome this problem is through the addition of a polymer such as polyethylene glycol (PEG) on the surface of the AuNP. PEG is known to be biocompatible and non-immunogenic, reducing the cytotoxicity and prolonging the half-life of nanoparticles (Lipka *et al.*, 2010). Alternatively surface ligands such as peptides have shown to improve stability, biocompatibility and solubility and most importantly employ cell-targeting. The accumulation of gold nanoparticles in tumours after systemic administration is also attributed to the enhanced permeability and retention effect (EPR). Angiogenesis often occurs at the site of tumour development. This creates a "leaky" region of vasculature, inducing the EPR effect. Blood vessels in the tumour could contain gaps up to 600 nm between the adjacent epithelial cells which allows for higher concentration of nanoparticles accumulation as compared to normal tissue (Arvizo *et al.*, 2011).

Taking all the above into consideration, it is clear that once nanoparticles prove to have the potential of being used as a diagnostic or as treatment, it needs to tested in an *in vivo* system.

1.11. The analysis of gold nanoparticle uptake and distribution

The evaluation of the uptake and distribution of gold nanoparticles can be analysed by various techniques (Hillyer & Albrecht, 2001). For evaluating organ distribution, including the kinetics of nanoparticle accumulation and excretion; radioactive labelling analysis, instrumental neutron activation analysis (INAA), inductive coupled plasma-mass spectroscopy (ICP-MS) and atomic absorption spectroscopy (AAS) (Mohamed Anwar & Halim, 2012) are common techniques used. INAA and ICP-MS are commonly used for the quantification of gold in tissue samples (Khlebtsov & Dykman, 2011).

Widely used techniques used to study the cellular uptake of nanoparticles are microscopy and flow cytometry. Flow cytometry allows for the fast quantification of nanoparticle uptake however does not provide an insight into the subcellular localization of nanoparticles as do electron microscopy. For the purpose of identifying and evaluating the localization of gold nanoparticles as well as their structural and elemental analysis, electron microscopy is the preferred and most commonly chosen technique.

1.12. High resolution transmission electron microscopy

In high resolution transmission electron microscopy (HRTEM), an electron beam is transmitted through an ultrathin biological sample, typically < 100 nm thick. In essence an image is formed from the electron interaction. This imaging technique can be used to determine the crystallinity and morphology of gold nanoparticles, the intracellular structure of biological material as well as the uptake mechanisms within cells (Lucocq & Gawden-Bone, 2010; Sperling *et al.*, 2008). This can be done with a thousand times smaller resolution than light microscopy could provide (Goodhew *et al.*, 2000)

Immunogold staining for antigen localization on ultrathin sections is one of the traditional uses of gold nanoparticles in transmission electron microscopy (TEM). With this technique subcellular structures are stained with gold nanoparticles functionalized to antibodies specific

to the antigen exposed on the surface of the ultrathin section. Gold nanoparticles possess a high electron density and can be easily detected under TEM (Lucocq & Gawden-Bone, 2010).

1.13. Aims and objectives

The aim of this research is to investigate the localization of three nanoparticle/peptide conjugates (AuNP-p.C, AuNP-p.L and AuNP-p.14) in cells and tissues of an *in vitro* and *in vivo* colorectal cancer model using high resolution transmission electron microscopy (HRTEM).

With this general aim in mind the three main objectives considered in this investigation were as follows:

1. To optimize and establish a colorectal cancer animal model using the AOM/DSS method

2. To evaluate the specific binding and localization of peptide-gold nanoparticles conjugates to colorectal cancer tumours compared to non-colorectal cancer using HRTEM.

3. To investigate the specific binding and localization of peptide-gold nanoparticles in cancer cell lines using HRTEM.

1.14. Thesis Scope

Chapter one begins the literature review, which provides an overview of colorectal cancer carcinogenesis, carcinogen-induced animal models, the diagnosis of CRC, the background to cancer screening peptides, gold nanoparticles and their cellular uptake mechanisms. Finally, aims and objectives are discussed to bring the project into context and assist in the elucidation of the methadology to be used throughout this investigation.

Chapter two provides a comprehensive description of the final methods and materials used during this investigation

Chapter three provides the reader with visual representation of all data obtained as well as interpretation of the data and discussion of the results obtained.

Chapter four provides the reader with the final conclusions and possible improvements to the project.

Chapter five accounts for all references in this dissertation

CHAPTER TWO: METHODS AND MATERIALS

2.1. Materials and methods

All the chemicals were of reagent grade and were used without further purification. Distilled water was further purified using Mili-Q reagent grade system. All glass wear was cleaned using aqua regia.

Azoxymethane (AOM)	Sigma-Aldrich
Dextran sodium sulphate (DSS) (5 kD)	Sigma-Aldrich
Paraformaldehyde	Agar scientific
Glutaraldehyde	Agar Scientific
Molecular grade ethanol	Spellbound solutions
LR White resin	Agar Scientific
DMEM	ATCC
FBS	Lonza
EMEM	Sigma-Aldrich
NAA	Lonza
Trypsin	Lonza
DMSO	Sigma Aldrich
300-mesh carbon-copper grids	SPI Supplies

2.2. Solutions and buffers

- **1 M phosphate buffer (PB)** - 3.1 g of $NaH_2PO_4.H_2O$, 10.9 g of Na_2HPO_4 (anhydrous) in 1 L MiliQ water (Stored up to 1 month, at 4°C, pH 7.4).
- **1 x phosphate buffer saline (PBSA)** - 8 g NaCl, 0.2 g KCl, 1.44 g Na_2HPO_4, 0.24 g KH_2PO_4 in 1L MiliQ water (Stored up to month, at 4°C, pH 7.4)
- **Cocktail fixative (Tissue)** - 2.5% glutaraldehyde and 2% paraformaldehyde in phosphate buffer saline (PB) at pH 7.4.
- **Cocktail fixative (Cell culture)** - 2.5% glutaraldehyde and 2% paraformaldehyde in phosphate buffer saline (PBS) at pH 7.4.
- **DMEM complete medium:** 10% FBS (5 mL), fill up with DMEM in sterile 50 ml tube. Complete medium was stored at 4°C

- **EMEM complete medium:** 10% FBS (5 mL), 1% NEAA (500 µL), fill up with EMEM in sterile 50 ml tube. Complete medium was stored at 4°C
- **Cryopreservation medium**- 20% FBS, 5% DMSO to respective growth media. Make fresh.
- **50% (v/v) Ethanol.** Ethanol (5 mL) was made up to 10 mL with dH_2O.
- **70% (v/v) Ethanol.** Ethanol (7 mL) was made up to 10 mL with dH_2O.
- **90% (v/v) Ethanol.** Ethanol (9 mL) was made up to 10 mL with dH_2O.
- **Resin: Ethanol (1:1).** LR White (100 µL) was mixed with an equal amount of absolute ethanol (100 µL).

2.3. Gold nanoparticles and characterisation

Colloidal gold nanoparticles were synthesized by Mintek (Randburg, South Africa). The respective AuNPs were conjugated to three peptides (p.C, p.L and p.14) through streptavidin-binding at Minpeptide (Randburg, South Africa). Table 2 lists the peptide-gold nanoparticle conjugates. The size, morphology, UV-vis absorption peak were determined by the manufacturer. To validate the product supplied, the size and morphology were analysed using the HRTEM. No data regarding their size and surface charge in solution was provided; this was obtained using the dynamic light scattering technique (DLS) and zeta potential (ZP).

Due to a confidential agreement, the sequences of the peptides are not mentioned here.

Table 2: Peptide-gold nanoparticle conjugates

Peptide name	**Peptide sequence**
p.C	
p. L	
p.14	

2.3.1. High resolution transmission electron microscopy

Electron micrographs were obtained using a JEOL JEM 2100 LaB_6 (NMMU) microscope. The samples were prepared by placing 1 part of the colloidal solution (AuNPs dispersed in dH_20) in 1 part of 99.9% absolute ethanol onto a 300-mesh carbon copper grid. In transmission

electron microscopy (TEM), an image is formed from the interaction of high energy electrons transmitted through the specimen. The image presents areas of mass-thickness contrast; where areas of higher density and thickness appear darker in contrast whilst areas of low density and thickness appear lighter in contrast. This provides information on the size and morphology of gold nanoparticles (AuNP) and biological structures (Miller & Lines, 1988; Wang, 2000).

2.3.2. Energy dispersive X-ray spectroscopy

Samples were analysed in the HRTEM equipped with energy dispersive X-ray spectroscopy (EDS, X-Max 80, Oxford Instruments) detector. This technique provided elemental and chemical analysis of nanomaterial being probed (Wu *et al.*, 2013). The interaction of electron beam on the sample produces X-rays that are characteristic to the elements present within the sample. The HRTEM samples (see section 2.3.2) have been analysed by EDS.

2.3.3. Dynamic light scattering and zeta potential

Dynamic light scattering (DLS) and zeta potential (ZP) measurements were performed on Zetasizer Nano using a Size and Zeta folded cell: DTS1060 at room temperature (RT) (Malvern Instruments). DLS characterizes the hydrodynamic radii (HD) of particles in solution (i.e. the inorganic core, as well as the surface modification). It is based on the measurement of light being scattered as a laser passes through a colloidal solution undergoing Brownian motion (at a constant temperature). By analysing the scattered light intensity as a function of time, this generates diffusion coefficients which are mathematically linked to the particle size and size distribution. ZP technique measures the movement of the charged particles in an electric field. This value is a useful in determining the stability of the suspension (i.e. large negative or positive zeta potential indicates better stability) and understanding nanoparticle-cell interactions (Wang *et al.*, 2009). Each sample was measured in triplicate and the mean value reported.

2.4. *In Vitro* Studies

2.4.1. Routine cell culture maintenance

Human epithelial colorectal adenocarcinoma (Caco-2, HT-29) and hepatocellular carcinoma (C3A) cell lines were cultured in 10 cm culture dishes. The Caco-2 and HT-29 cell lines were

maintained in Dulbecco's Modified Eagle's Medium (DMEM), supplemented with glutamine and 10% (v/v) fetal bovine serum (FBS). The C3A liver cell line was maintained in Eagles Minimum Essential Medium (EMEM) supplemented with 1% non-essential amino acids (NAA) and 10% (v/v) FBS. All solutions were stored at 4°C and pre-warmed to 37°C in a water-bath prior to use. The cells were maintained in 5% $C0_2$ at 37°C (Celis *et al.*, 2005).

Cells were subcultured after 70-80% confluency. Subculturing was performed by removing media from the attached cells. Cells were washed with 10 mL phosphate buffered saline (PBSA) and trypsinized by adding 1 mL of 0.25% trypsin (v/v). Cell detachment was facilitated by placing the dish in the 37°C incubator for 5-10 minutes. The cells were re-suspended in 2 mL of media, after which the cells were plated (1:3 ratio) into new culture (Ng *et al.*, 2010; Schrand *et al.*, 2010).

2.4.3. Storing and thawing of cell culture

Confluent cells (70-80%) were detached from the cell culture dishes as described above in section 2 and centrifuged for 5 minutes at 500g. The pellet generated was re-suspended in 3 mL fresh complete media. Cells were microscopically counted using a haemocytometer and trypan blue. $1x10^6$ cells/ml were re-suspended in cryopreservation media. The cryo-tubes were placed at -80°C (Celis *et al.*, 2005).

2.4.4. Cell culture nanoparticle exposure

HT-29, Caco-2 and C3A cell lines were seeded in 10 cm culture dishes at a cell density of $3x\ 10^5$/ml and grown to a desired confluence. The cells were treated with AuNP-p.C, AuNP-p.L and AuNP-p.14 (1 nM) for 6 hours, at 37°C as established by the cellular uptake kinetics of 14 nm AuNPs in Hella cells previously evaluated by Chithrani *et al.* (2006).

2.4.5. TEM cell preparation

The preparation of biological samples (i.e. cells and tissue) for electron microscopy requires several stages which includes sample washing, fixation, dehydration, embedding, sectioning and analysis as seen in Figure 2.1. The cell preparation for electron microscopy was performed as described by Schrand *et al.* (2010), with minimal modification.

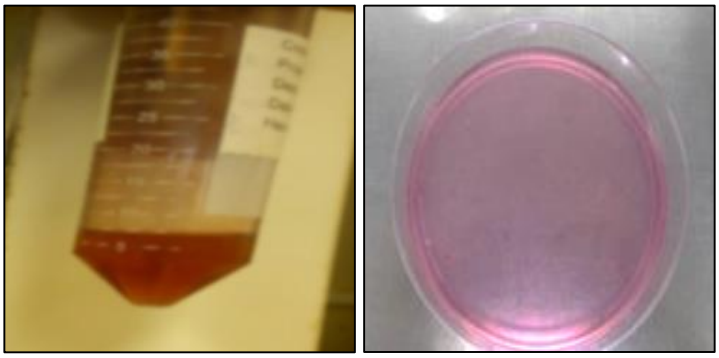

A. Grow cells and treat cells with AuNPs

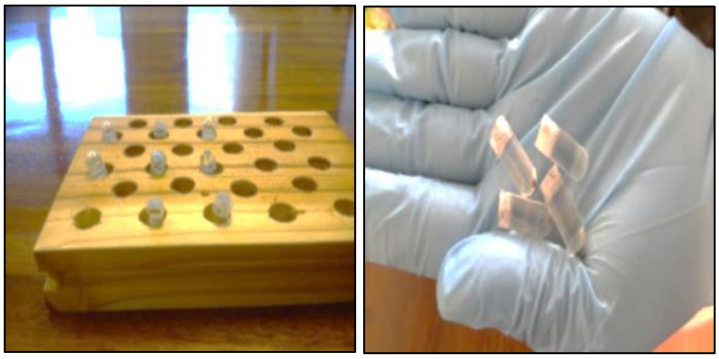

B. Rinse, pellet, dehydrate and embed cells in LR White resin

C. Polymerization in oven at 60°C

D. Trim and section samples ultramicrotome (NMMU)

E. Image in JEOL JEM 2100 LaB6

Figure 2.1: Overview of sample preparation process (A-E). (A) Grow and dose cells with AuNPs, (B) Cell processing (rinse, pellet, dehydrate, embedding), (C) Curing, (D) Trim and sectioning of sample, and (E) Imaging with HRTEM.

2.4.5.1. Sample washing and harvesting

Before sample harvesting, the cell monolayer should be washed thoroughly. This is important as the surface may contain a variety of unwanted deposits such as media components, free/unattached gold nanoparticles, cellular debris or contaminants. If these deposits are not removed prior to centrifugation and fixation procedure, the material may get permanently fixed to the specimen surface. The cells monolayer as described in section 2.4.4, was washed three times with PBSA (pH 7.4) at room temperature (RT). 1 mL of PBSA was added to each cell dish and scraped off the plate. The cell suspension was transferred to eppendorfs and centrifuged at 1000g to generate a cell pellet (Ng *et al.*, 2010; Schrand *et al.*, 2010).

2.4.5.2. Fixation

The first critical stage of biological preparation for electron microscopy is fixation. The aim of fixation is to preserve the structure of the cell (shape, size, 3D dimensional organisation, cellular activity) and protecting the cell from structural deformation that could occur during dehydration, embedding, sectioning and staining (Newman *et al.*, 1982, 1983). After cell harvesting, the PBSA was removed from the eppendorf tubes and replaced with a fixative cocktail of 2.5% glutaraldehyde and 2% paraformaldehyde in PBSA at pH 7.4. This was left to incubate for 2 hours at RT (Schrand *et al.*, 2010).

2.4.5.3. Dehydration

The aim of the dehydration process is to remove water from the biological sample by the addition of increasing concentrations of an organic solvent such as ethanol (Hayat, 1974; Newman & Hobot, 1999). This is essential as the biological sample may be embedded in a water-insoluble resin such as LR White. After the fixation process, samples were washed thrice with PBSA (pH 7.4) for 10 min. This was carried out in order to minimize the possible reaction of fixative and dehydration reagent. The dehydration procedure was carried out with a series of 50, 70, 90 and 100% (2x) molecular grade ethanol concentrations for 15 min each (Hayat, 1974).

2.4.5.4. Embedding in LR White resin

LR White is a polyhydroxy aromatic acrylic resin introduced by Causton (1984). After the dehydration procedure, the cell pellets were gradually infiltrated with LR White resin and 100% ethanol at a ratio of 1:1 for 1 hour (Hayat, 1974). The cell pellets were transferred to a

BEEM gelatin capsule. The gelatin capsules were filled with pure LR White resin to generate a positive meniscus and covered to exclude oxygen. Geletin capsules were incubated for 4 hours at 4°C. This allowed for complete infiltration before polymerization at 60°C for 38 hours. Post-fixation/staining with heavy metals were avoided to prevent possible interference (i.e. heavy metal artefacts) with the identification of gold nanoparticles (Hillyer & Albrecht, 2001; Jong *et al.*, 2010).

2.5. *In vivo* Studies

2.5.1. Ethical approval

This study was approved by the Animal Research Ethics Committee (REC-A) of Nelson Mandela Metropolitan University (A13-SCI-ZOO-013).

2.5.2. Animal maintenance

Healthy adult male Wistar laboratory rats (15 weeks of age) were obtained from North West University animal institute (South Africa). Animals were housed five per cage. The Animals were maintained at a temperature of 22°C (± 3°C), with a 12 hour light and 12 hour dark cycle. All animals were fed standard commercial rat chow and given distilled water *ad libitum.*

2.5.3. Animals and experimental design

After weaning, 35 male Wistar rats were assigned to six groups, five experimental groups and one control group.

- Experimental group (group 1, group 2 and group 3; n=6) were assigned to the colorectal cancer induction experiment and treated with AuNP-p.C, AuNP-p.L and AuNP-p.14. Experimental group 1 was subjected to the AOM/DSS method 1. Experimental group 2 and 3 were subjected to AOM/DSS method 2.
- Experimental group (Group 4 and 5; n=6) were maintained as healthy rats treated with AuNP-p.C and AuNP-p.14. This was performed as a means to evaluate and gain a firm understanding of AuNP biodistribution/accumulation between tumour-bearing and

non-tumour bearing (healthy) rats. An additional healthy group treated with AuNP-p.L was not carried out due to animal breeding constraints and timing.

- Control group (group 6; n=5) were healthy and did not receive any treatment. Table 2 lists the Animal experimental procedure and design

After rats were sacrificed (see section 2.6.5) and tissue was collected (see section 2.6.7), all tissue pieces from animal groups were processed for HRTEM (section 2.6.8). Due to time constrains, tissue from AOM/DSS method 1 (colon, rectum, pancreatic and kidney), Group 4 (kidney) and Group 5 (liver) were analysed. See Figure 2.2, a schematic diagram of research design.

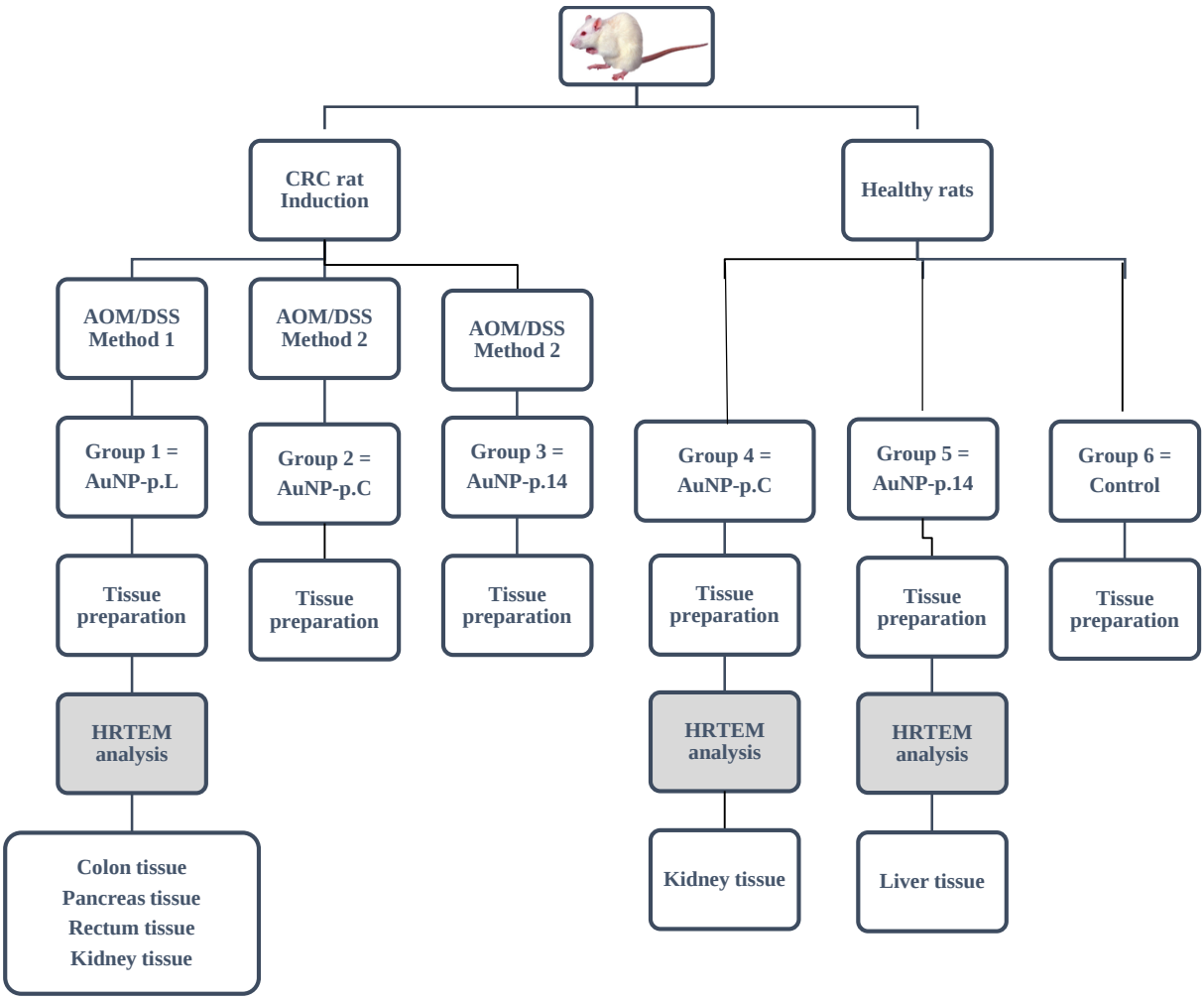

Figure 2.2: Schematic diagram of research design and electron microscopy evaluation

2.5.4. Induction of colorectal cancer

2.5.4.1. AOM/DSS method 1

Wistar rats were assigned to three CRC induction-experimental groups. Group 1 was subjected to the AOM/DSS method 1, and later treated with AuNP-p.L. This was done in conjunction with a control group (group 6). The control group represents a healthy non-treated AuNP study.

The standard AOM/DSS method 1 procedure was followed as described by Thaker *et al.* (2012). Male Wistar rats (n=6) were given a single intraperitoneal injection of AOM (12 mg/Kg body weight) at week 1 followed by 1 week of distilled water. At week 3, 3 cycles of DSS (1 cycle included 2% DSS with a molecular weight of 5kDa for 1 week followed by distilled water for 2 weeks) were administrated. At the end of week 11, the animals were monitored for an additional 2 weeks before all animals (group 1) were intravenously injected with AuNP-p.L (week 14) and sacrificed 24 hours later. Each week the body weights of the animals were recorded. Figure 2.3 illustrates the AOM/DSS method 1 procedure.

14 Week	AOM	dH_20	DSS	dH_20	DSS	dH_20	DSS	dH_20	dH_20	AuNP
Group 1 n=6	W1	W2	W3	W4+5	W6	W7+8	W9	W10+11	W12+13	W14

Figure 2.3: AOM/DSS method 1: The establishment of a CRC rat model. W1-14:Weeks 1-14, AOM–Azoxymethane injections (grey box), DSS- 2% dextran sodium sulphate administration (black box), dH_20- normal distilled water (White box), AuNP- AuNP injection (red box).

2.5.4.2. AOM/DSS method 2

The decision was made to alter the AOM/DSS protocol by Thaker *et al.* (2012) to assist in obtaining colorectal cancer tumours. Wistar rats assigned to CRC induction-experimental groups (group 2 and 3) followed the AOM/DSS method 2 procedure.

Wistar rats (n=6) were given a single intraperitoneal injection of AOM (12 mg/Kg body weight) at week 1 followed by 1 week of distilled water. At week 3, 2 cycles of DSS (1 cycle included 2% DSS with a molecular weight 5kDa for 1 week followed by distilled water for 2 weeks) were administrated. After the 2 cycles of DSS treatment, both groups were given a second AOM injection (12 mg/kg body weight) at week 9. This was followed by the administration of a 2 cycles of DSS at week 12 and 15. At the end of week 17, the animals

were monitored for an additional 2 weeks before all animals (group 2 and group 3) were intravenously injected with AuNP-p.C (group 2) and AuNP-p.14 (group 3) and sacrificed 24 hours later. Each week the body weights of the animals were recorded. Figure 2.4 illustrates the AOM/DSS method 2 procedure.

20 Week	**AOM**	**dH_20**	**DSS**	**dH_20**	**DSS**	**dH_20**	**AOM**	**dH_20**	**DSS**	**dH_20**	**DSS**	**dH20**	**dH_20**	**AuNP**
Group 2 + 3 n=6	**W1**	**W2**	**W3**	**W4+5**	**W6**	**W7+8**	**W9**	**W10+11**	**W12**	**W13+14**	**W15**	**W16+17**	**W18+19**	**W20**

Figure 2.4: AOM/DSS method 2: The establishment of a CRC rat model. W1-14:Weeks 1-14, AOM-–Azoxymethane injections (grey box), DSS- 2% dextran sodium sulphate administration (black box), dH_20-distilled water (White box), AuNP- AuNP injection (red box).

Due to time constraints of this study and the high cost in the development and maintenance of inducing colorectal cancer, the AOM/DSS method 2 was initiated after the third and last DSS cycle of the AOM/DSS method 1. The rats were then injected with AuNP/peptide conjugates after the AOM/DSS treatment for evaluating the nanoparticle targeting efficiency. This was done in conjunction with a control group (group 6).

Currently there are no sensitive and specific techniques available other than colonoscopy to detect early stage colorectal cancer. Colonoscopy would be difficult in this research setup, thus rats were treated with gold nanoparticles and sacrificed at the time expected to develop colorectal cancer. According to the literature, the percentage of weight loss is a sign of colorectal cancer development and was used in this study. Other signs such as rectal bleeding and diarrhoea are indicative of a late stage in the development of colorectal cancer and was therefore not applicable in this study.

2.5.5. Sacrifice of rats

Prior to necroscopy, final weight measurements were taken before individual rats were given an intramuscular injection of Ketamine (100 mg/kg body weight) as an anaesthetic. After no signs of sensory reflexes, blood was withdrawn via cardiac puncture which caused hypovolumic death. All rats were laid on their ventral side exposed on a cutting board. The abdomen was covered with 70% ethanol to prevent hairs from contaminating abdomen content. Forceps were used to grasp the midline of the abdomen. A small incision was then made to

expose the peritoneum. This incision was extended to both sides of the abdomen along the costal margin. Scissors were used to cut through pelvis for exposing the rectum (Thaker *et al.*, 2012). Figure 2.5., shows the necroscopy process

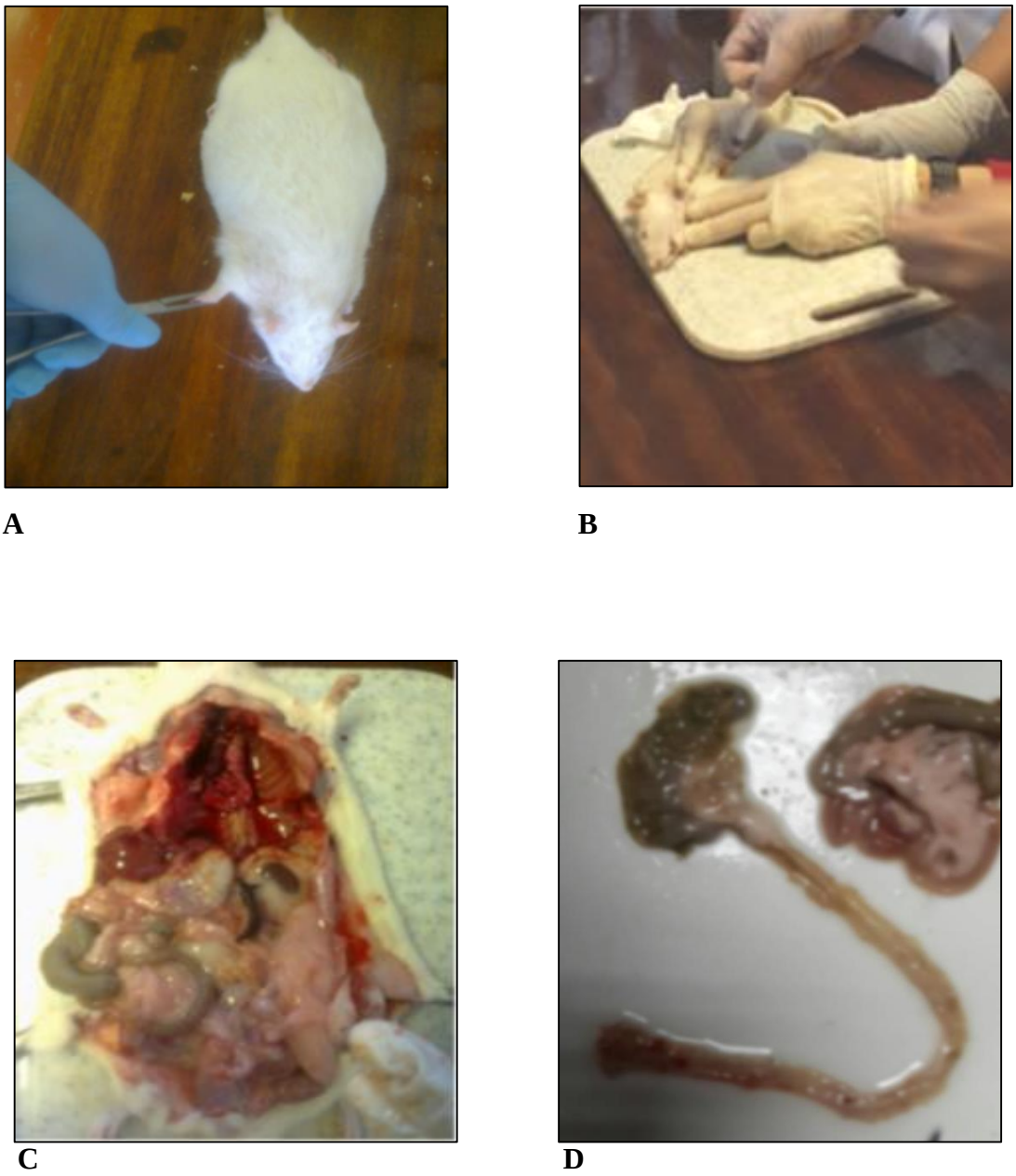

Figure 2. 5: Rat necroscopy: (A) The tendon reflex is used to assess the level of consciousness of the rat, (B) Blood is removed from heart before necroscopy procedure, (C) The abdomen is cut exposing the abdominal viscera, and (D) The removal of the large intestine.

2.5.6. Tissue harvesting

After sacrificing the animals, the colon, small intestine, spleen, kidney, liver, brain, heart and lungs were rapidly removed to prevent autolysis. Due to time constraints of this research project, emphasis was placed on the colon in particular. The colon was removed, cut open longitudinally along the main axis and washed with saline. All tissue were cut into 1 mm^3 pieces.

2.5.7. TEM tissue preparation

Tissue pieces (1 mm^3) removed from the sacrificed animals was prepared for TEM as established in section 2.4. The tissue pieces were fixed in a mixture of 2.5% glutaraldehyde and 2% paraformaldehyde in 0.075 M phosphate buffer (PB) pH 7.4, at room temperature (RT) overnight. After three washes with phosphate buffer, the tissue pieces were dehydrated at room temperature through a series of ethanol concentrations at 50, 70, 90 and 100% (2x). After dehydration, tissue pieces were gradually infiltrated with LR White resin and 100% molecular grade ethanol at a ratio of 1:1 for 1 hour at room temperature. The samples were then embedded in pure LR White resin for 4 hours before polymerization at 60°C for 38 hours (Ng *et al.*, 2010; Skepper & Powell, 2008). Post-fixation/staining with heavy metals were avoided to prevent possible interference (i.e. heavy metal artefacts) with the identification of gold nanoparticles (Hillyer & Albrecht, 2001; Jong *et al.*, 2010).

2.5.8. Ultramicrotome methodology for sectioning ultrathin sections.

The aim of tissue processing is to embed the tissue in a solid medium firm enough to support the cells/tissue and give it sufficient rigidity to enable thin sectioning. The cell and tissue samples chosen were sectioned using the LKB standard glass knifemaker (Ng *et al.*, 2010; Skepper & Powell, 2008). Before the sections were cut, glass knives were prepared, as seen in Table 3.

Ultrathin sections (80-100 nm) were cut with using the Reichart UltracutE ultramicrotome. Sections were transferred to 300 – mesh carbon copper grid.

Table 3: Glass knife preparation for ultrathin sectioning (Adapted from Wickens (2012))

MAKING GLASS KNIVES	
STEP	**ACTION**
1.	A 25mm wide x 200mm long x 6mm thick glass strip was washed with soapy water and/or alcohol to remove grease and dirt. This was allowed to dry on a paper towel.
2.	The scoring bar was pushed in and the score selector was set to parallel lines.
3.	The breaking knob was pushed counter clockwise.
4.	The glass strip was placed on the LKB machine, resting against a white plate and pressing against a black stud.
5.	Whilst the glass was held in place, the clamping head was lowered until it touched the glass strip. The clamp was then securely tightened.
6.	The scoring shaft was then pulled to create a scoring line in the glass.
7.	The breaking knob was then turned clockwise until the glass broke.
8.	The glass knob was immediately returned to fully counter-clockwise position and clamping head lifted.
9.	The glass square was then placed turned counter clock wise from its original cutting position using the fork. The glass was then placed between two glass holders (“corners”).
10.	A securing knob was used to clamp the square glass between tow forked holders.
11.	The damping pad was lowered until it touched the glass.
12.	The scoring bar was then turned to 25 mm thickness and glass square scored by pulling the scoring shaft outwards.
13.	The breaking knob was then turned clockwise slowly until the square broke.
14.	The clamping head was immediately lifted, scoring shaft returned and breaking knob turned clockwise.
15.	The glass knife was then released carefully the fork.
Sectioning at 80- 100 nm	
1.	A glass boat was made with silver tape and secured with dental wax/ nail paint
2.	The glass knife was placed securely in the knife holder
2.	The boat was filled with clean filtered water to a level below the knife edge
3.	The knife holder was fitted into the cutting arm and fastened tightly.
4.	Once the alignment was set, the macro-feed wheel was brought forward to almost touch the knife
5.	The rough sample block was lightly trimmed 1 um at a time.
6.	Once the sample block face was smooth, the auto wheel was turned on and the ultramicrotome cut 70-100 nm sections into the water bath (Silver- Gold ultrathin sections)
7.	When a suitable ribbon was cut, the sections were stretched with chloroform fumes.
8.	The sections were then lifted onto TEM grids using forceps and allowed to dry for 30 minutes

2.5.9. Statistical analysis

Results were statistically analysed using Student's t-test in conjunction with GraphPad Prism 6.0. P value <0.05 was considered significantly different

CHAPTER THREE: RESULTS AND DISCUSSION

Results and discussion consists of three sections; characterization of AuNPs (section 3.1), *In vitro* studies (section 3.2) and *In vivo* studies (section 3.3).

3.1. Characterization of AuNPs

3.1.1. Aims of investigation

The characterisation of nanoparticles (i.e. size, shape and surface functionalization) are critical issues for the delivery of nanoparticles as well as understanding their cellular interactions (Jiang *et al.*, 2009). The peptide-AuNP conjugates were obtained from Mintek. The size and morphology of the AuNPs were characterised by researchers at Mintek. For control and observation purposes, this was confirmed using HRTEM (as described in section 2.3).

3.1.2. Results

3.1.2.1. Characterisation by high resolution transmission electron microscopy

Table 3 summarises the measurements of the three peptide-AuNP conjugates. The majority of AuNPs were spherically shaped with an average size of 14 nm. A general view over the TEM grids confirmed the presence of stable particles. As depicted in Figure 3.1 (A, B and C), the core of the AuNPs possess a dark contrast with resolved lattice fringes (indicated by lattice fridges). It was observed that AuNP-p.C (Figure 3.1.A) and AuNP-p.14 (Figure 3.1.C) were surrounded by a transparent layer indicated by a black arrow. No such layer was observed for AuNP-p.14 (Figure 3.1.B).

3.1.2.2. Characterisation by dynamic light scattering and zeta potential

As depicted in Table 4, the HD of AuNPs-p.C and AuNPs-p.L and AuNPs-p.14 were found to be approximately 11 nm larger than the core diameters measured by HRTEM (as described in section 3.1.2.2). The data further reports low polydispersity index, high zeta potentials and a negative surface charge.

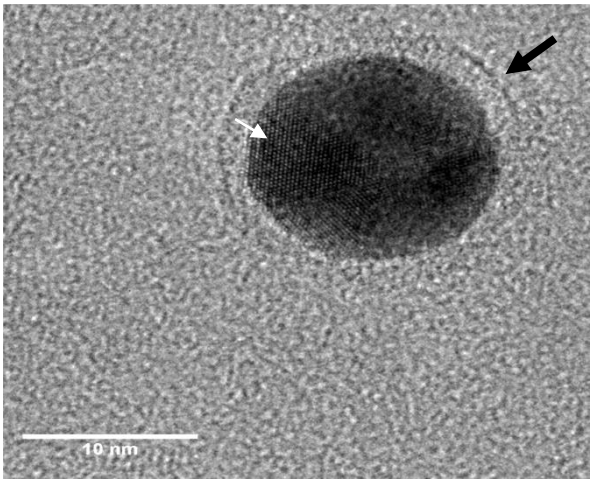

A

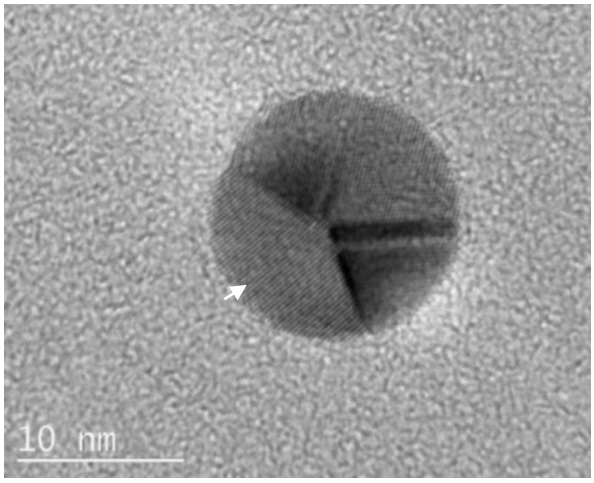

B

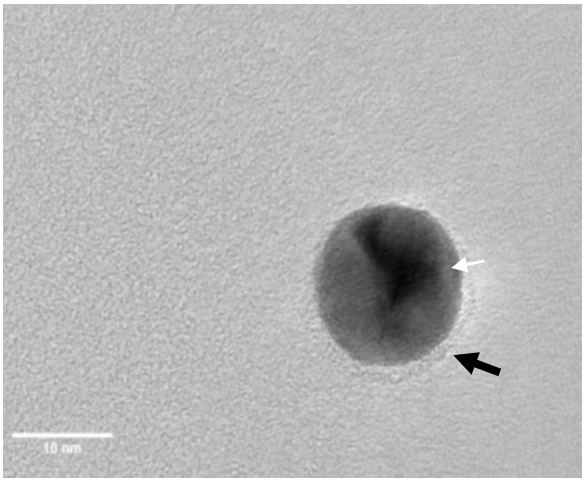

C

Figure 3. 1: TEM Bright field (BF) images of (A) AuNPs-p.C, (B) AuNPs-p.L and (C) AuNPs-p.14. Black arrow indicates layer around AuNP. White arrow indicates lattice frindges.

Table 4: The characterisation of gold nanoparticles attached to peptide

AuNP-peptide	DLS (nm ± std dev)	TEM (nm ± std dev) (as supplied)	Zeta-Potential (m.V)	Suspension media (as supplied)	UV-vis Absorption peak	Polydispersity
AuNP-p.C	25.30 ± 0.115	14±3 nm	-22.40	MiliQ water	521 nm	0.196
AuNP-p. L	24.63 ± 0.77	14±3 nm	-42.3	MiliQ water	523 nm	0.399
AuNP-p.14	24.40± 0.055	14±3 nm	-67.6	MiliQ water	524 nm	0.148

3.1.3. Discussion

Gold nanoparticles have attracted considerable attention in biological applications. The unique properties exhibited by gold nanoparticles are attributed to their physicochemical characteristics. Determining these characteristics could play a vital role in understanding how gold nanoparticles associate with the living system (Jiang *et al.*, 2009).

HRTEM micrographs confirmed spherical shaped AuNPs showing lattice fringes indicative of good structural quality gold nanoparticle conjugates (Wang, 2000). Due to mass-thickness contrast AuNPs are of darker contrast, however, biomolecules are of low density and therefore appear "electron transparent" (i.e. unless stained with heavy metals) (Chatterjee *et al.*, 2012). In this study, it seems that the lattice fridges of AuNPs seen in Figure 3.1 (A and C) cannot be clearly seen. It is suggested that this could be due to the layer/coating surrounding the AuNP-p.C and AuNP-p.14. This layer is presumed to be the peptide molecules conjugated to the AuNPs. The lattice fridges of AuNP-p.L are the most visible as seen in Figure 3.1.B, which could be a result of no layer/coating being observed around the nanoparticle structure. The absence of the layer/coating surrounding AuNP-p.L (Figure 3.1.B) could be due to sample preparation of peptide-AuNP conjugates for TEM (as demonstrated in section 2.3) or the application of the TEM beam. This is just a suggestion; such an observation is best studied using DLS, which has confirmed a size difference of approximately 11 nm for all three AuNPs due to peptide conjugation. DLS and zeta potential measurements further report that the AuNP solution is well dispersed, free from aggregation or agglomeration (Yin Win & Feng, 2005).

3.2. *In vitro* studies

3.2.1. Aim of investigation

Mazyambe (2013) demonstrated that binding of quantum dot nanoparticles conjugated with p.C was highly specific towards Caco-2 and HT-29 cells, while quantum dot nanoparticles conjugated with the p.L peptide demonstrated specificity towards HT-29 cells. The objective of this section was to further investigate the uptake and localization of nanoparticles (gold nanoparticles) conjugated with these peptides. A third peptide (p.14), which was demonstrated to have selectivity towards colon cancer cells (Wang *et al.*, 2012), and which was not part of the Mazyambe study was also included in the current study. While Mazyambe's study used

flow cytometry to study the binding of the fluorescent nanoparticles to the cells, the current study used HRTEM to study the uptake and localization of the AuNP/peptide conjugates (AuNP-p.14, AuNP-p.C and AuNP-p.14) in colorectal cancer cells (Caco-2 and H-T29) and liver cancer cells (C3A). The cells were exposed to the AuNP/peptide conjugates and the uptake and localization of the nanoparticles were then studied using HRTEM as described in section 2.4.5.

3.2.2. Results

Electron micrographs of HT-29 cells treated with AuNP-p.14 (Figure 3.2.A, B) and AuNP-p.C (Figure 3.3.A, B) displayed features which included increased cell volume, intact nucleus, distortion of all subcellular organelles, a disruption of the plasma membrane and the release of cellular components into extracellular space.

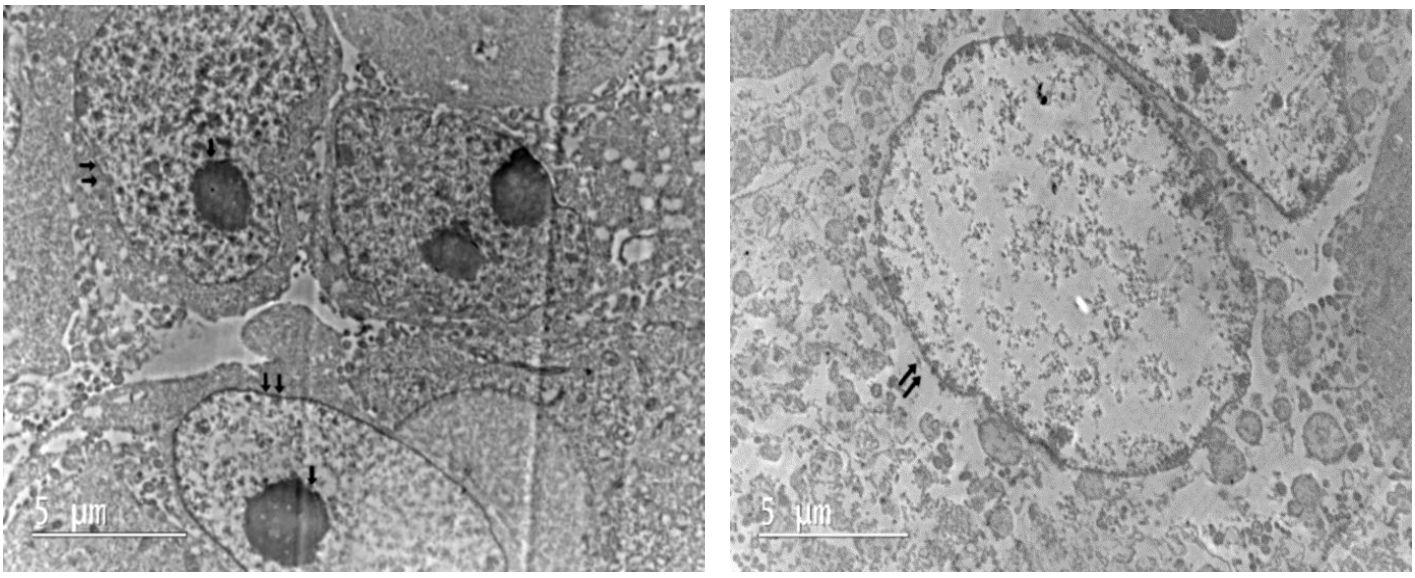

A **B**

Figure 3. 2: TEM (BF) micrographs of HT29 cell line treated with AuNPs-p.14 (n=1). (A, B) Two arrows indicate the cell membrane; single arrow indicates the cell nucleus.

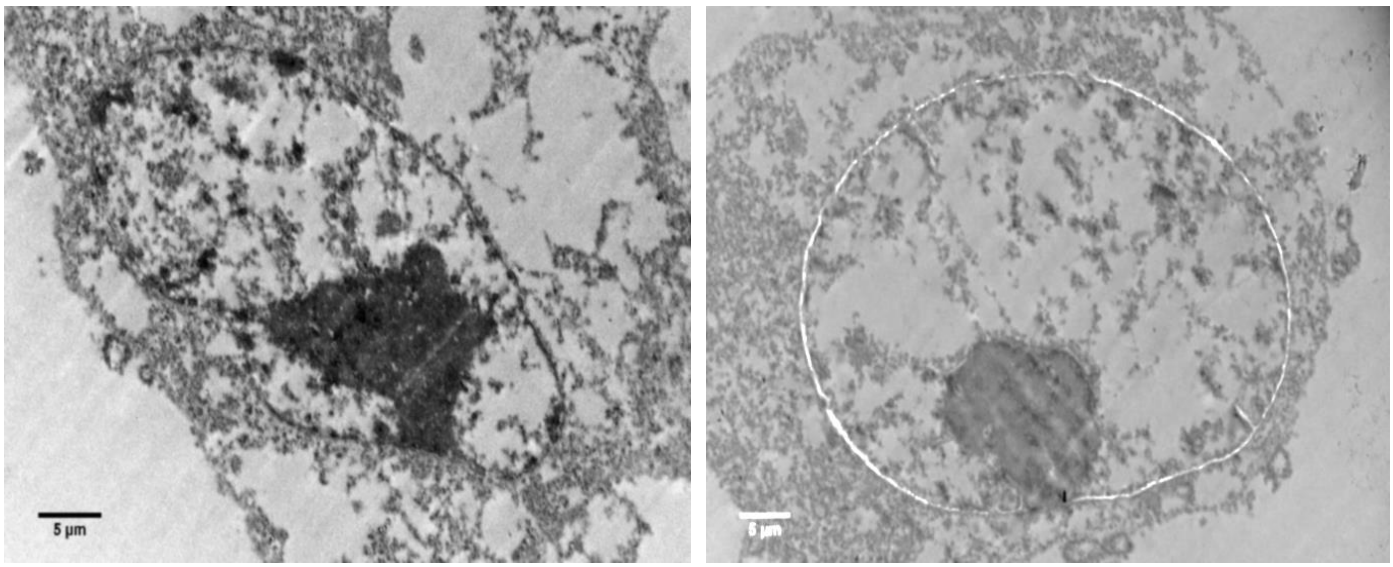

A B

Figure 3. 3: TEM (BF) micrographs of HT29 cell line treated with AuNPs-p.C (n=1). (A, B) Two arrows indicate the cell membrane and single arrow indicates the cell nucleus.

3.2.3. Discussion

It is empirical to the aims of this study to be able to identify AuNPs but also permit the visualization of cellular components and organelles. This can only be seen if the cells were suitably prepared for electron microscopy. If prepared appropriately, the expectation is that the appearance of cells should approximate that of living cells. This assumption finds support from the mass-basis TEM procedure adapted from Schrand *et al.* (2010).

However, in this study the fine cellular structure of the cells could not be preserved. HT-29 cells as depicted in Figure 3.2 (A,B) and Figure 3.3(A,B) displayed features which included increased cell volume, intact nucleus, distortion of all subcellular organelles, a disruption of the plasma membrane and the release of cellular components into extracellular space. These features were all indicative of necrotic cell death. Necrotic cell death occurs when cells are exposed to extreme variance in physiological conditions (Fernandez-Prada *et al.*, 1998; Majno & Joris, 1995; Proskuryakov *et al.*, 2003). In an attempt to improve the quality of sample preservation, several parameters from the methodology (as described in section 2.4.5) were identified for optimization. Table 5 lists the parameters for optimal cell preservation. No

selective targeting and localization of AuNPs to HT-29 cells were observed, however, these findings cannot be confirmed as of yet.

Table 5: Parameters for optimal cell preservation.

1.	**Cell harvesting**
a.	Cell scraping/cell trypsinization
b.	Centrifugation speed
2.	**Fixation of cells**
a.	Fixative type
b.	Concentration
c.	*In situ* fixation
d.	pH
e.	Osmolarity
3.	**Dehydration of cells**
a.	Time
b.	Temperature
4.	**Embedding of cells**

3.2.3.1. Cell harvesting

The cells were harvested from the plastic surface of the cell culture dish before fixation as described by Schrand *et al.* (2010). In this study, the cell scraping technique was chosen. This technique can potentially cause more damage to cell integrity compared to trypsinization (Magee *et al.*, 1958). On the other hand trypsinization can possibly interfere with membrane associated proteins and therefore also the AuNP/peptide conjugates if the nanoparticles are localised to the to the membrane. Due to uncertainty of AuNP localization (intracellular or membrane association), trypsinization was abandoned and the cell scraping technique was used. It is also possible that the cells optimal growth conditions were compromised before cell fixation. We therefore propose to investigate an alternative technique known as *in situ* fixation. In this way, the cell monolayer in culture dish goes undisturbed whilst being preserved (Ryan & Hart, 1986).

Another contribution to cell damage prior to the fixation step could be the high centrifugal forces during centrifugation (in this study 1000*g* for 5 minutes was used). There is no well-defined speed to centrifuge cells into a pellet for TEM processing. Schrand *et al.* (2010) have utilized 1000*g* in their studies, whilst Nativo *et al.* (2008) used 5000*g* and have reported good results. To confirm whether centrifugation plays a significant role in cell damage, HT-29 cells were grown under optimal conditions, detached from the cell culture dish and centrifuged at two centrifugation speeds (500*g* and 1000*g*). The cells were then re-suspended and cell viability was assessed by trypan blue staining. No significant cell damage occurred at these speeds. A less compressed cell pellet was generated at 500*g*, which could potentially cause difficulty with washing, dehydrating and embedding. There is also a concern that centrifugation forces could contribute to unwanted interactions between the nanoparticles and cells (Schrand *et al.*, 2010). A lower centrifugal force with pre-shaped BEEM capsule tips would circumvent this confrontation and ease specimen collection and orientation in future research.

3.2.3.2. Fixation of cells

The electron micrographs for *in vitro* studies demonstrate unsuccessful preservation of HT-29 cells. All indications of fixative artefacts. The pH, osmolarity, temperature, length of fixation and concentration of fixatives are critical factors in determining the quality of fixation (Hayat, 1974; Newman & Hobot, 1999). It is therefore essential that the method of fixation needs to be in line with the objectives of the study (Hayat, 1974; Newman & Hobot, 1999). For the best results; a combination of paraformaldehyde and glutaraldehyde (Karnovsky's fixative) is generally used. This has proved to be successful in preserving both ultrastructure and immunogenicity in cells or tissue (Griffiths, 1993; Newman *et al.*, 1982). Paraformaldehyde is able to penetrate cells/tissue very quickly, reacting with uncharged primary amine groups and aromatic amino acid residues. It is able to stabilize the protein structure but gives poor preservation of ultrastructure. Glutaraldehyde penetrates tissue more slowly and reacts with amino acids, aromatic, carboxyl, amidozole and sulfhydryl groups. It has the ability to preserve ultrastructure better than any known fixative. Glutaraldehyde also increases the permeability of the tissues to the embedding medium (Hayat, 1974). For immunocytochemical experiments, cells/tissues are often fixed in paraformaldehyde (2-4%) and glutaraldehyde (0.1-0.2%) in a PBSA solution. However, small amounts of glutaraldehyde in the fixative would not achieve

adequate ultrastructural detail (Takizawa *et al.*, 2003). To achieve ultrastructural detail, Schrand *et al.* (2010) used a 2.5% glutaraldehyde/formaldehyde fixative. In this study, a combination of 2.5% glutaraldehyde and 2% paraformaldehyde in PBSA solution was used to preserve the cultured cell samples. Immunogenicity may therefore have been compromised in this study as a higher glutaraldehyde percentage was used (Mühlfeld *et al.*, 2007). The pH levels in the different structural compartments of the cell vary significantly (Hayat, 1974). To achieve the best structural for preservation, cells and tissues must be kept at a pH between 7.2 and 7.4, with a physiological osmolarity of ~280 mOsm (Loqman *et al.*, 2010). Throughout this experiment, the pH of the phosphate buffer saline was kept at 7.4. However, the osmolarity of the fixative was disregarded and should be looked into as it has shown to play a direct influence on the appearance of the cell structure

Post-fixation with heavy-metals (e.g. osmium tetroxide) is usually required as it further stabilizes the fine structure already maintained by aldehydes but also acts as an electron stain, imparting a high contrast to biological material (Hayat, 1974; Sabatini *et al.*, 1964; Schrand *et al.*, 2010). In this study, the post-fixation step was omitted to prevent the electron stain and to elucidate the identification of gold nanoparticles present in biological material. If contrast is required it could be corrected for through image processing techniques, thickness during sectioning and staining with heavy metals (lead citrate, uranyl acetate, etc.) as demonstrated by Schrand *et al.* (2010). It is certainly possible that omission of the post-fixation step with heavy metals could play a part in the preservation of the cells. This needs to be investigated further.

3.2.3.3. Dehydration and embedding of cells

Acetone is known to interfere with LR White resin polymerization (Hayat, 1974; Schrand *et al.*, 2010; Skepper & Powell, 2008). It is for this reason that ethanol was chosen as the organic solvent for the dehydration of the cell pellet. In this study, dehydration was gradually carried out with a 50, 70, 90 and 100% (2x) ethanol for 10 minutes each. This procedure is essential as LR White resin is water-insoluble. However, ethanol is a lipid solvent and dehydration must be accomplished as rapidly as possible to avoid leaching of lipids from cellular components. According Philimonenko *et al.* (2002), 5-15 minutes of dehydration each is sufficient. Embedding the cell sample provides additional support. It allows sufficient handling of the

sample when sectioning. LR White resin was chosen for its low viscosity, low toxicity and low extraction rate compared to alternative resins (Newman & Hobot, 1999).

3.2.3.4. Sectioning

To gain the resolution required to view individual nanoparticles and ultrastructural detail, a section thickness less than 100 nm is often required (Schrand *et al.*, 2010). Section thickness lower than between 80 nm could not be obtained with the ultramicrotome equipment used in this study, and as a result the sections were of poor quality. Problems with variations in section thickness and vibrations also added to the poor quality of the sections. It was thought that a way to reduce the thickness of the sample would be to mount the section on a naked grid. This idea failed as stability of the section under the electron beam was reduced.

Taking all the above into consideration, TEM sample preparation requires several stages, which include sample washing, fixation, dehydration, embedding. Each stage in sample preparation has a great impact in the quality of the resulting cell sample.

3.3. *In vivo* studies

3.3.1. Aim of investigation

AOM/DSS is a recognised method to induce colorectal cancer. AOM is a carcinogen that induces tumours in the colon whilst DSS causes inflammation. The severity of inflammation hastens the development of colorectal tumours. This can be monitored by weight loss and pathological features such as rectal bleeding and diarrhoea (Perše & Cerar, 2005).

The aim of this investigation was to establish and optimize a colorectal cancer animal model using the AOM/DSS procedure. This animal model was used to investigate the localization of AuNP/peptide conjugates (AuNPs-p.C, AuNPs-p.L and AuNPs-p.14) to colorectal tumours using HRTEM.

3.3.2. Results

3.3.2.1. The induction of colorectal cancer in rat model

AOM/DSS method 1:

Group 6 (Control) showed a higher average body weight than Group 1 (AOM/DSS method 1), however the difference was not significant until the day of AuNP treatment (P=0.0176). This is illustrated in Figure 3.4.

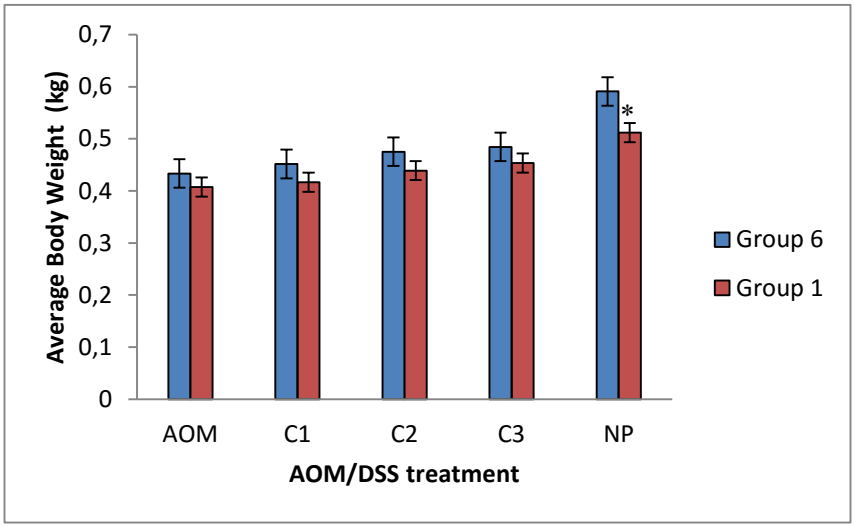

Figure 3. 4: Average body weight (kg) at different time points between group 6 (Control, n=5) and group 1 (AOM/DSS method 1, n=6). AOM denotes the body weight taken on the day of AOM injection, C1, C2 and C3 denotes the weight taken at the end of cycle 1, 2 and 3. NP denotes the weight taken before AuNP injection.

Wistar rats given the AOM/DSS method 1 treatment (Group 1) were sacrificed 24 hours after AuNP-p.L injection. Pathological features which include a bloody stool and diarrhoea were not observed. No animals died prematurely. After each rat sacrifice, the colon was inspected for the presence of neoplastic lesions. This was done with the assistance of Dr. Ernest. Fredericks, a Gastroenterologist in private practice in Port Elizabeth (Greenacres Hospital). Majority of suspected lesions were excised from the distal colon for tissue processing as described in section 2.6.7. From the same site of excision, a second excision was made and the suspected lesions were removed and placed in 10% formalin. Samples were sent to Ampath, Greenacres Laboratory (South Africa) for analysis. Histopathological findings indicated suspected lesions were highly inflamed but no colorectal cancer present. See Figure 3.5.B for excision sites of inflamed colon tissue.

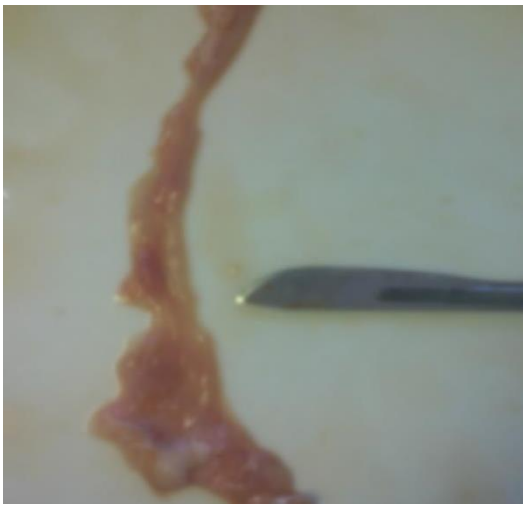

A

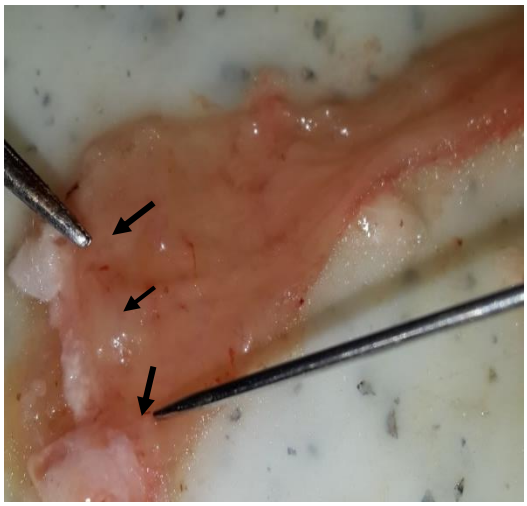

B

Figure 3. 5: Examination of colon. (A) Image of colon showing no lesions, (B) Excision sites of rat colon lesions indicated by black arrows.

AOM/DSS method 2:

No significant difference in body weight between group 6 (control) and group 2 and 3 (AOM/DSS method 2) were observed as seen in Figure 3.6.

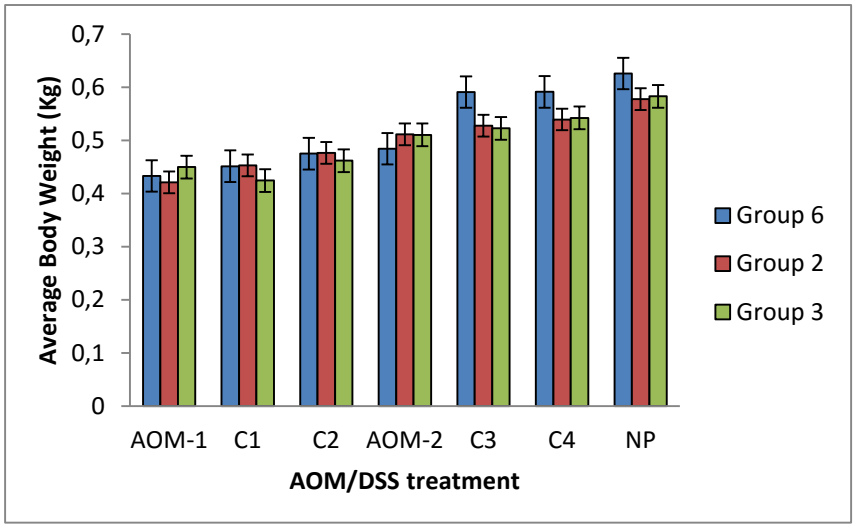

Figure 3. 6: Average body weight (kg) at different time points between group 6 (control, n=5), group 2 and group 3 (AOM/DSS method 2, n=6). AOM-1, AOM-2 denotes the body weight taken on the day of AOM injection, C1, C2 and C3 denotes the weight taken at the end of cycle 1, 2 and 3. NP- denotes the weight taken before AuNP injection.

Wistar rats in group 2 and 3 were subjected the AOM/DSS method 2. Pathological features such as a bloody stool and diarrhoea were not observed. The animals were sacrificed 24 hours after their AuNP-p.C (group 2) and AuNP-p.14 (group 3) injection. No animals died prematurely. The colon was inspected for the presence of neoplastic lesions. No lesions could be identified in AOM/DSS method 2 (as seen in Figure 3.5. A)

Taking all the above into consideration, animals in AOM/DSS method 1 (Group 1) experienced significant weight loss on the last week before AuNP treatment, however did not present any pathological features (except for inflammation) and neoplastic lesions. Animals given the AOM/DSS method 2 (Group 2 and group 3) experienced no weight loss or pathological features and did not present neoplastic lesions.

3.3.2.2. HRTEM analysis of tissue

This study describes the evaluation of tissue samples from inflamed colon (Figure 3.7), rectum tissue (Figure 3.8), pancreatic tissue (Figure 3.8) and kidney tissue (Figure 3.9) after being subjected to AOM/DSS method 1 treatment. Healthy liver tissue (group 5) (Figure 3.10) and healthy kidney tissue (group 4) (Figure 3.12) were also evaluated after being subjected to AuNP/peptide treatment. The tissue samples were taken 24 hours after the nanoparticles were injected into the animals. TEM micrographs of each tissue were examined according to the criteria specified by the Hayat (1974) and investigated for the presence of gold nanoparticles.

Colon tissue taken from inflamed regions is shown in Figure 3.7. Electron micrographs revealed collagen fibres (Cf) as seen in Figure 3.7.A. The inflamed colon tissue presented irregular shaped nuclei (N) with an intact nuclear membrane. Adjacent to the nuclear membrane, were dense chromatin masses as seen in Figure 3.7 (A, B, C). Cellular components were observed and are presumed to be mitochondria (Mi) (Figure 3.7.A, B), rough endoplasmic reticulum (RER) (Figure 3.7. B) and Golgi body (G) (Figure 3.7.C). To elaborate further, cellular objects labelled as mitochondria took on a circular outline, a common shape as reported by Grimstone (1968). However, this can only be presumed as their internal structure, cristae, could not be seen.

Further staining procedures would be needed to confirm the above observation. The arrangement of layers/membranes with the appearance of granular material (ribosomes) attached were presumed to be rough endoplasmic reticulum (RER), see Figure 3.7.B. As seen in Figure 3.7.C, the Golgi body seen adjacent to the nucleus has been observed to be a large collection of membranous layers closely packed together, covered with ribosomes. According to Hayat's criteria, a well preserved rough endoplasmic reticulum and Golgi body should appear to have flattened cristae, uniformly arranged and intact membranous layers with attached ribosomes. No gold nanoparticles were observed.

A

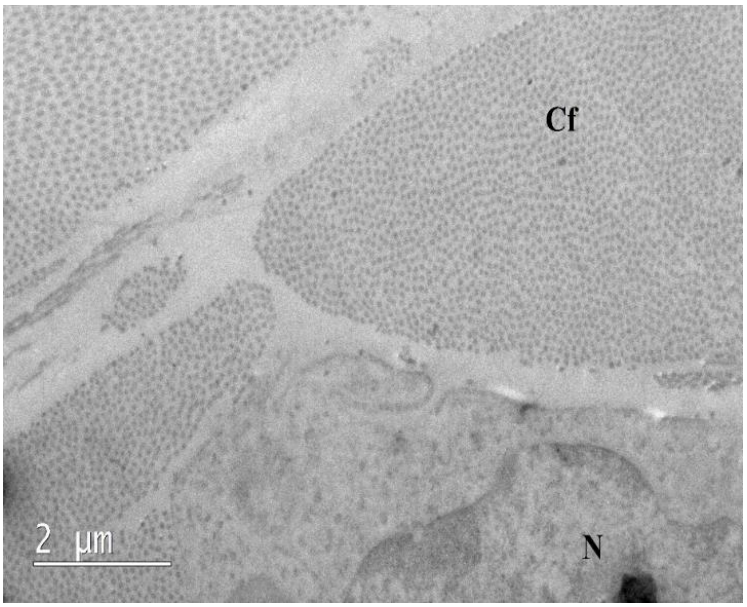

B

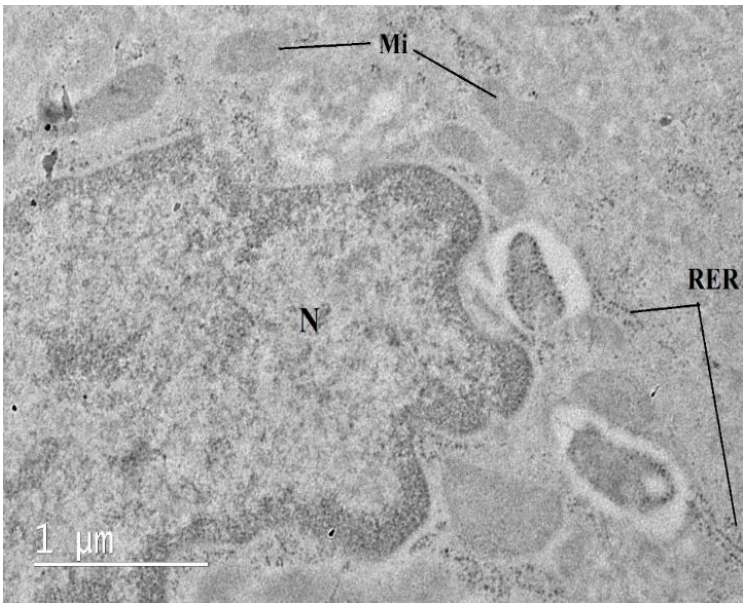

C

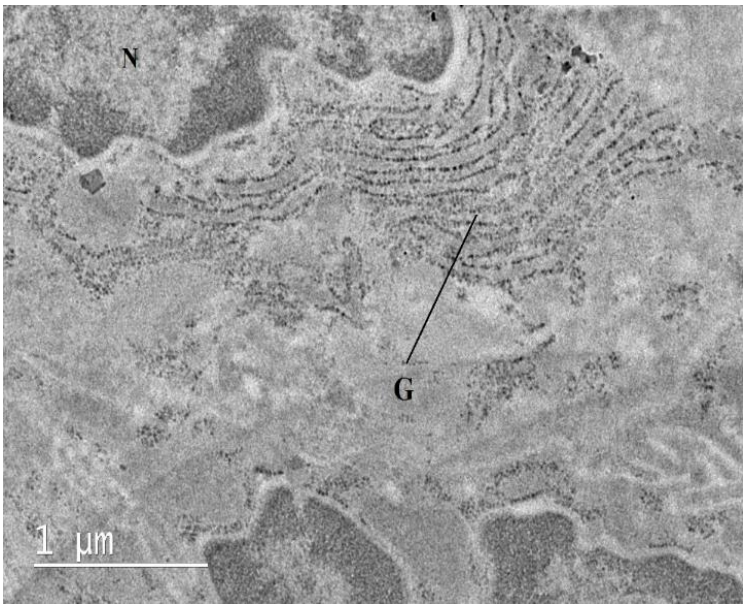

Figure 3. 7: TEM (BF) micrographs of colon tissue from inflamed regions of animals treated with AOM/DSS method 1, taken 24 hours after intravenous injection of AuNP-p.L. (Cf)- Collagen fibres, (N) Nuclei, (RER) Rough endoplasmic reticulum, (Mi) Mitochondria and (G) Golgi body.

Tissue from the rectum is shown in Figure 3.8. Figure 3.8.A and B illustrate microvilli (Mv), interdigitations (I) and tight junction indicated by a black. Other subcellular constituents such as endoplasmic reticulum, Golgi body and lysosomes were not visible. No gold nanoparticles were observed.

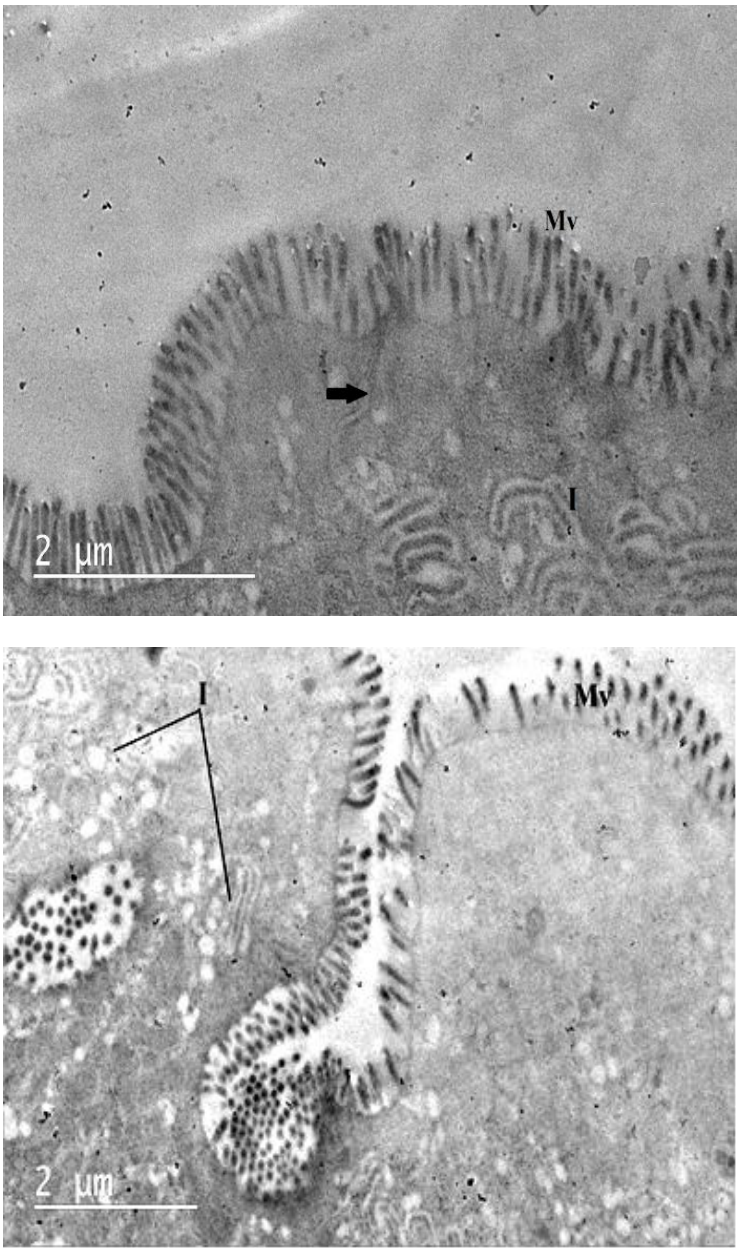

Figure 3. 8: TEM (BF) micrographs of rectum tissue of AOM/DSS method 1, taken 24 hours after intravenous injection of AuNP-p.L. (Mv) Microvilli, (I) Interdigitations and a tight junction (black arrow).

Pancreatic tissue is shown in Figure 3.9.A. Cellular components depicted in Figure 3.9.A, were presumed to be numerous zymogen granules (ZG) and smooth endoplasmic reticulum (SER). These cellular components corresponded to cellular components reported by Kitagawa and Ono (1986). The zymogen granules were of irregular sizes whilst the smooth endoplasmic reticulum was seen as intact membranes unattached to ribosomes surrounding the zymogen granules. No gold nanoparticles were observed.

A

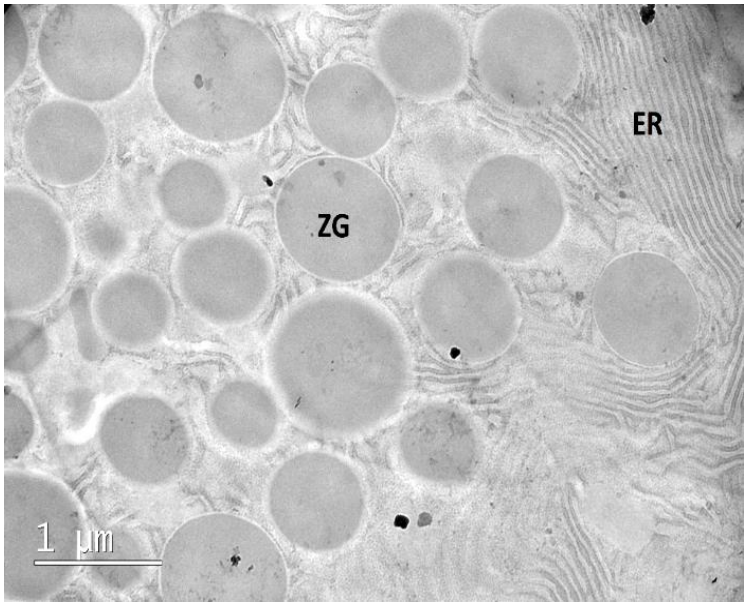

Figure 3.9: TEM (BF) micrograph of pancreatic tissue of animals treated with AOM/DSS method 1, taken 24 hours after intravenous injection of AuNP-p.L. (ZG) Zymogen granules and (SER) Smooth endoplasmic reticulum.

Kidney tissue is shown in Figure 3.10. Cellular components depicted in Figure 3.10.A, revealed numerous densely packed, long mitochondria (Mi) orientated vertically among a layer of basal membrane (BM) and an intact nuclear membrane. These cellular components corresponded to the ultrastructural detail reported by Verlander (1998).

A

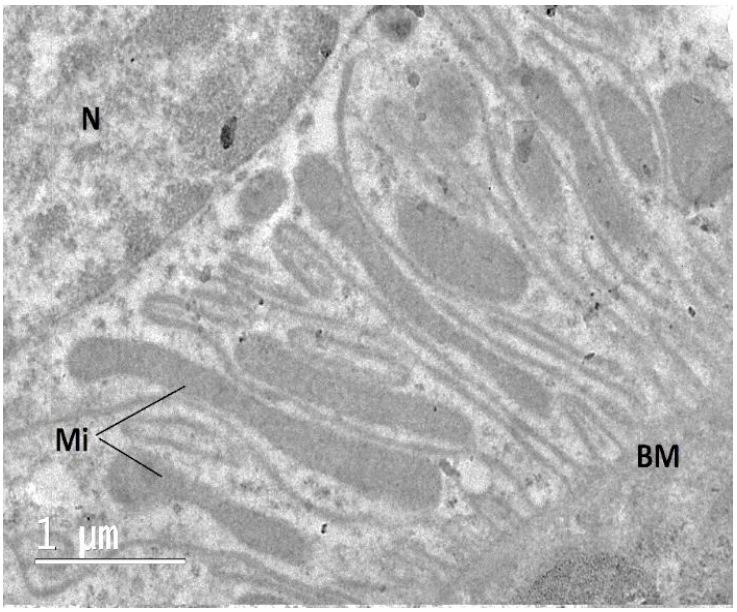

Figure 3.10: TEM (BF) micrographs of kidney tissue of animals treated with AOM/DSS method 1, taken 24 hours after intravenous injection of AuNP-p.L. (N) Nucleus, (Mi) Mitochondria and (BM) Basal membrane.

Healthy liver tissue treated with AuNP-p.14 from group 5 is shown in Figure 3.11. Cellular components depicted in Figure 3.11.A, are likely to be rough endoplasmic reticulum (RER) and numerous irregular shaped mitochondria (Mi) showing intact cristae. A tight junction can be observed as indicated by two black arrows. These cellular components are based on similar ultrastructural studies reported by Kühnel (2003). The evaluation of Figure 3.11.B and C revealed the presence of electron-dense particles in cytoplasmic background surrounding mitochondria, as indicated by one black arrow. High resolution images as seen in micrograph B and C assisted in further characterizing the structure of the electron dense particles. However, resolution of particles could not be further resolved as seen in Figure 3.11.C. In order to elucidate the identity of these structures, additional TEM studies were performed with energy-dispersive-X-ray (EDS) spectrum analysis. These structures could not be identified by EDS spectrum analysis to contain gold. EDX spectrum results not shown.

A

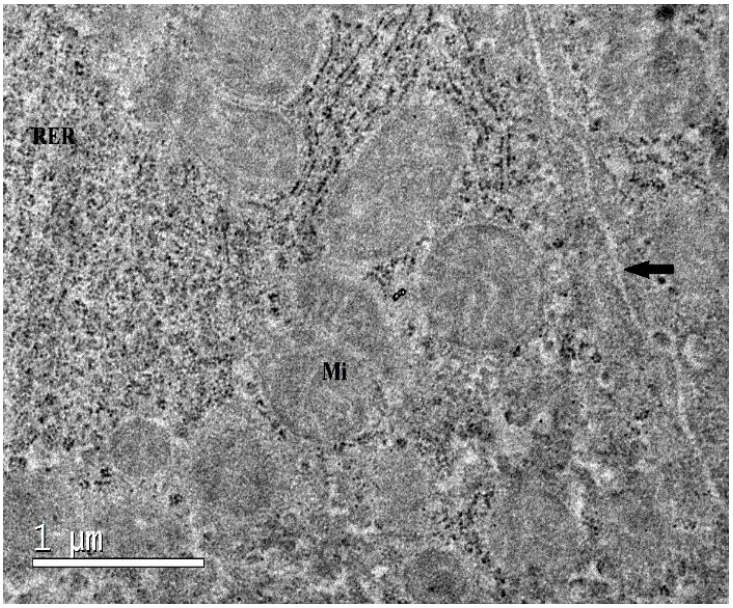

B

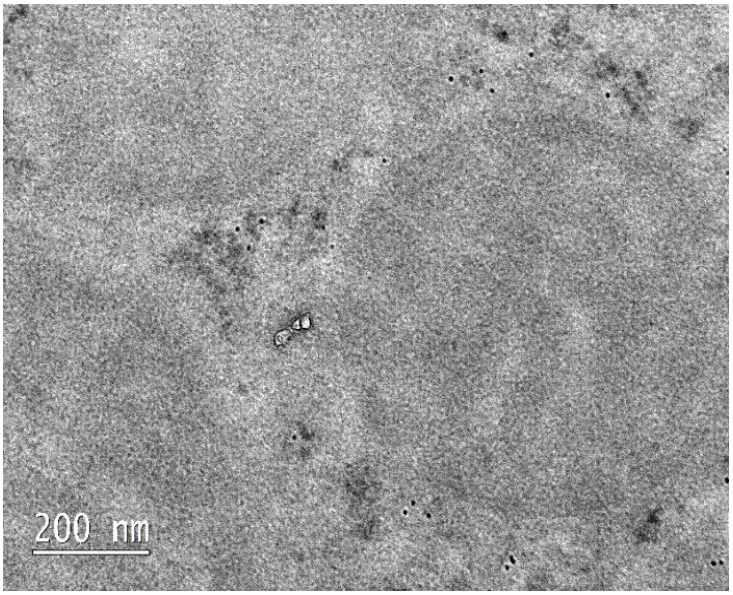

C

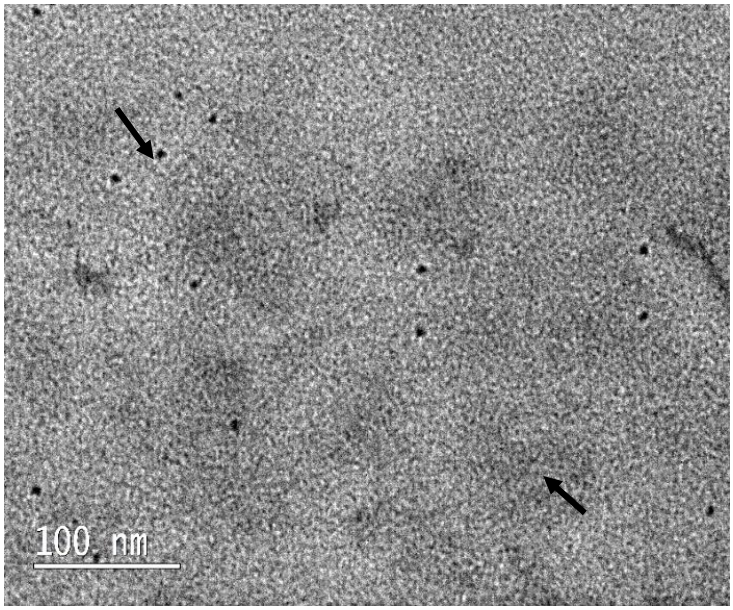

Figure 3.11: TEM (BF) micrographs of healthy liver tissue from group 5, taken 24 hours after intravenous injection of AuNP-p.14. (RER) Rough endoplasmic reticulum, (Mi) Mitochondria and Tight junction (two black arrows). At higher magnification, electron dense particles indicated by single black arrow.

Healthy kidney tissue treated with AuNP-p.C from group 4 is shown in Figure 3.12. The bright field micrograph seen in Figure 3.12.A indicated the presence of electron-dense particles. A high angle annular dark field image (HAADF) was recorded with the scanning transmission electron (STEM) microscope as seen in Figure 3.12.B. This technique is highly sensitive to atomic mass. A bright contrast is indicative of elements with higher density such as metals. However this technique does not efficiently confirm the presence of gold elements (Kempen *et al.*, 2013). EDS spectroscopy identified the presence of gold. EDS spectrum results not shown.

A

B

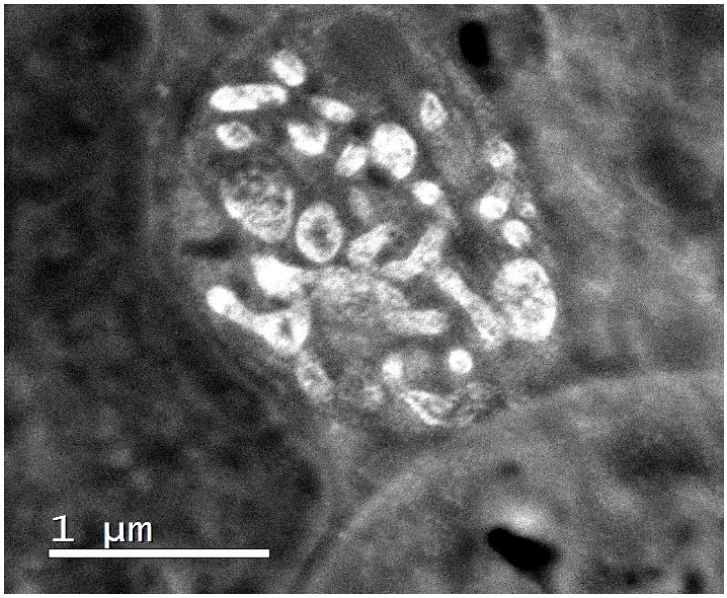

Figure 3.12: TEM (A) BF and (B) High angle annular dark field (HAADF) micrograph of heathy kidney from group 4, taken 24 hours after intravenous injection of AuNP-p.C.

3.3.3. Discussion

Most rodents, including rats, do not spontaneously develop colorectal cancer and are therefore predominantly used as a colorectal cancer model (Corpet & Pierre, 2005). When using single or multiple injections of AOM, colon tumour development has shown a low tumour incidence with a 7 to 9 month latency period (Neufert *et al.*, 2007; Tanaka *et al.*, 2003). However, with the follow-up treatment of DSS, tumour development could take as little as 7 to 10 weeks (Thaker *et al.*, 2012). The objective of this study was first to establish and optimize a colorectal cancer rat model for the investigation of specific targeting and localization of peptide-gold nanoparticle conjugates (AuNPs-p.C, p.L and p.14) towards colorectal cancer tumours. This study was the first CRC induction to be investigated in our laboratory.

Between the two models investigated (AOM/DSS method 1 and AOM/DSS method 2), histopathological findings suggested suspected lesions identified from AOM/DSS method 1 protocol were inflamed and were not neoplastic contrary to findings of Thaker *et al.* (2012). The methods applied in this study therefore failed to induce colonic neoplasms in the rat model. Due to time constraints of this project and the high cost in the development of inducing colorectal cancer in rats, the animals given the AOM/DSS treatment were subjected to the AuNP/peptide treatment before they were to be sacrificed. When CRC was not observed in any AOM/DSS treated rats, results were interpreted to reflect a situation where nanoparticles have been injected for screening purposes. This study suggests that AuNP conjugated with the peptides used in this study will not give false negatives.

Rats given DSS have been shown to either develop acute or chronic colitis (Perše & Cerar, 2012). Chronic inflammation through long term DSS administration was shown to hasten the development of colonic malignancies. It has been stated that the relative weight loss is a surrogate measure of severity of colitis (Thaker *et al.*, 2012). As depicted in Figure 3.4, throughout the AOM/DSS treatment, the control group (group 6, n=5) showed a higher average body weight than the group 1 (AOM/DSS method 1, n=6) but the difference was not significant until the day of AuNP treatment (P=0.0176). No significant difference in body weight between control group (group 6, n=5) and group 2 and 3 (AOM/DSS method 2, n=6) were observed, as seen in Figure 3.6. Apart from no significant weight loss, other symptoms of colitis severity

include a bloody stool and diarrhoea. These symptoms were not observed in the three experimental (group 1, group 2 and group 3) in this study.

Although some researchers have administered multiple injections of AOM to induce CRC, this study could not prove that the two treatments of AOM benefit CRC development more than the one treatment. This study rather suggests that AOM increases the chances of DNA modification whilst the severity of inflammation following the initiation determines the development of CRC. It seems as if the severity of the inflammation is determined by the molecular weight of the DSS. Therefore, in future it seems to be important that DSS with a higher molecular weight of 40-50 kDa needs to be used. According to Perše and Cerar (2012) tumour promoting effects of DSS is said to be influenced by various factors, which include the DSS administration and duration, manufacturer, animal species and microbiota. Research findings conducted by Suzuki *et al.* (2005) has shown that the tumour promoting effect of DSS is dose-dependent. The use of a DSS dosage above 1% contributed to an increase in inflammation of the colon resulting in the increase incidence of tumours. However, the tumour promoting role of DSS was not specified in regards to the various molecular weights of DSS.

According to the results of this study it also appears that, in the case of a minor inflammation, the body may develop a mechanism to combat the inflammation which may be the reason why there was no inflammation found in the rectum area of the rats in groups 2 and 3 (AOM method 2). The mechanism in which DSS works is still under investigation. A possible suggestion to the non-occurrence of inflammation within group 2 and 3 (AOM/DSS method 1) could be bacterial bioactivity capable of improving colonic damage. This is just a suggestion and can be investigated at a later stage in another study, using the tissues that were collected in this study.

In this study, all specified tissues (see section 2.6.6) were prepared for TEM visualization. Due to practical constraints not all tissue could be analysed. Tissue taken from control groups, group 1 (inflamed colon tissue, rectum, pancreas and kidney), group 5 (liver) and group 4 (kidney) were further analysed by HRTEM (see Figure 2.2).

Due to the unsuccessful induction of colorectal cancer, all experimental groups represent non-colorectal tumour animal models. This can provide us with the necessary information regarding the distribution/accumulation of nanoparticles in healthy tissues and organs. This study has evaluated the presence of gold nanoparticles in group 1 and 5 and has found no accumulation

of AuNP-p.L and AuNP-p.14, respectfully. This suggests that these nanoparticles are unable to target to healthy tissues. The accumulation/biodistribution of AuNP-p.C in the kidney of experimental group 4 suggests that the AuNP-p.C does not bind to healthy tissues and as a result have been cleared by the kidneys in the absence of a ligand which should be present if cancer was induced. For any diagnostic or therapeutic application, the absence of nanoparticles in healthy tissue and the removal of nanoparticles by renal clearance is preferred as this would imply that the AuNP/peptide conjugates exhibits a " safe behaviour" (Alric *et al.*, 2013).

CHAPTER FOUR: CONCLUSION AND FUTURE DIRECTIONS

4.1. Conclusion

Colorectal cancer (CRC) is the third most common cause of cancer-related deaths worldwide. Early colorectal cancer diagnosis is vital in reducing incidence and mortality. However, there is a need for the development of sensitive, specific and non-invasive screening tools for enhancing the detection of the disease. Complementing the knowledge of disease biomarkers, biomarker targeting molecules and nanotechnology can create a powerful diagnostic platform. Nanomaterials like gold nanoparticles have stimulated much interest in cancer research due to their unique physicochemical characteristics. Numerous studies have investigated the physicochemical characteristics (i.e. shape, surface charge, surface functionalization, concentration etc.) of these nanomaterials. However, a limited number of studies have dealt with their uptake and localization within cells and tissue utilizing HRTEM. This is an essential tool in understanding the interaction of all nanomaterials in an *in vitro* and *in vivo* model.

The aim of this dissertation was to investigate the uptake and localization of three AuNP/peptide conjugates (AuNP-p.C, AuNP-p.14 and AuNP-p.L) in an *in vitro* and *in vivo* CRC model using HRTEM. In this study we employed 14 ± 3 nm colloidal gold nanoparticles synthesized by Mintek (Randburg, South Africa) and attached respectfully to the three peptides (p.C, p.L and p.14) by Minpeptide (Randburg, South Africa). TEM micrographs confirmed the size and morphology of the AuNPs. The size and surface charge of the peptide-gold nanoparticle conjugates in solution were further characterized by DLS and zeta potential. These techniques verified that the spherical AuNPs were uniform in size and morphology and were attached to their respective peptides. The nanoparticle solutions were also found to be stable in dispersion.

In the present study, peptide-gold nanoparticle conjugates (AuNP-p.C, p.L and p.14) were investigated to achieve localization within cancer cell line (HT-29, Caco-2 and C3A). The cell sample underwent TEM preparation, which included sample washing, fixation, dehydration, and embedding. However, ultrastructural detail revealed signs of morphological alterations, which included changes in cell volume, subcellular organelle distortion, cellular leaking and plasma membrane disruption. Here, we were unable to demonstrate the localization of AuNPs

as a result of these findings. After studying the effects of the fixative and TEM preparation on the cell ultrastructure, we have identified additional steps and considered a different approach towards the handling of the biological samples for electron microscopy. In future, the in situ fixation approach, a low centrifugal force, the pH and osmolarity of fixative will be further investigated to avoid ultrastructural damage. It is possible that the omission of the post-fixation stage using heavy metals such as osmium tetroxide could have played a part in the preservation of cells. This will need to be investigated further. We can conclude that the findings of this study require modifications which would facilitate the selection of the best method to use for nanoparticle cell interactions.

An objective of this study was to establish a colorectal cancer rat model for the investigation of specific binding and localization of AuNP/peptide conjugates (AuNPs-p.C, p.L and p.14) towards colorectal cancer tumours. This study was the first to be investigated in our laboratory and could not address this objective. Despite this, the non-colorectal cancer animal models provided an insight into the distribution of AuNP/peptide conjugates in healthy tissue and organs. The optimization of a CRC animal model will be approached again in the future. Future research should use a DSS molecular weight of 40 kD. The type of food, source of DSS and susceptibility of animal model will be looked into as this could affect the severity of colitis and the induction of tumours. Overall, TEM preparations of chosen tissue samples were of adequate standard.

We presented an alternative approach to the preservation and visualization of TEM studies by omitting the post-fixation and staining of heavy metals. The results obtained surprisingly provided adequate contrast. However, in light of the aims of this study, the ability to determine the localization of AuNPs in different cellular compartments is essential. To obtain better quality preservation and contrast of cellular components, heavy metal fixation /staining would be necessary. Collectively, results suggest further research on electron microscopy cell/tissue preparation and the induction of colorectal cancer is warranted.

In conclusion, with the increase in nanomaterial research and production, research involving transmission electron microscopy exposes the nanoparticle localization and their interaction with other biological entities. This is an essential task needed to be performed, specifically for future medical applications in targeted diagnostics and drug delivery.

4.2. Recommendations for future work

In future, HRTEM results can be further validated by evaluating the biodistribution of gold in various organs using inductively coupled plasma mass spectrometry (ICP-MS). This technique gives an elemental analysis and therefore estimates the concentration of gold in each sample.

The following study presented an alternative approach to the preservation and visualization of TEM studies by omitting the post-fixation and staining of heavy metals. Although adequate contrast was achieved; unstained specimens require a low electron dose as a higher dosage could result in specimen damage. However this leads to a poor signal-to-noise ratio and noisy images. One of the ways that this could be improved would be cryo-electron microscopy. Imaging specimens at low ambient temperatures have been shown to reduce election damage as much as 6 fold compared to room temperatures. For future research, this would mean better imaging with a higher electron dosage.

4.3. Limitations

This study created awareness to various difficulties and limitations when using electron microscopy. The latter technique is the best for providing the necessary spatial resolution to visualize individual nanoparticles. However, this is a very time consuming (cell fixation, dehydration, resin embedding, TEM analysis) and low throughput process. This technique requires numerous images to be taken from a number of ultrathin sections to obtain significant results. TEM also requires the identification of nanoparticles from a small analysis volume which suggests that this technique is not suitable in determining the biodistribution of gold but would be adequate for determining the localization of gold within various tissue types. It can be suggested that TEM together with ICP-MS be used as complimentary tools in determining the systemic distribution and localization of gold within tissue

BIBLIOGRAPHY

Alric, C., Miladi, I., Kryza, D., Taleb, J., Lux, F., Bazzi, R., . . . Roux, S. (2013). The biodistribution of gold nanoparticles designed for renal clearance. *Nanoscale, 5*(13), 5930-5939.

Antonovych, T. T. (1981). Gold nephropathy. *Annals of Clinical & Laboratory Science, 11*(5), 386-391.

Armaghany, T., Wilson, J. D., Chu, Q., & Mills, G. (2012). Genetic alterations in colorectal cancer. *Gastrointestinal Cancer Research: GCR, 5*(1), 19.

Arvizo, R. R., Miranda, O. R., Moyano, D. F., Walden, C. A., Giri, K., Bhattacharya, R., . . . Mukherjee, P. (2011). Modulating pharmacokinetics, tumor uptake and biodistribution by engineered nanoparticles. *PLoS One, 6*(9), e24374.

Balasubramanian, S. K., Jittiwat, J., Manikandan, J., Ong, C.-N., Yu, L. E., & Ong, W.-Y. (2010). Biodistribution of gold nanoparticles and gene expression changes in the liver and spleen after intravenous administration in rats. *Biomaterials, 31*(8), 2034-2042.

Balogh, L., Nigavekar, S. S., Nair, B. M., Lesniak, W., Zhang, C., Sung, L. Y., . . . Bolton, B. (2007). Significant effect of size on the in vivo biodistribution of gold composite nanodevices in mouse tumor models. *Nanomedicine: Nanotechnology, Biology and Medicine, 3*(4), 281-296.

Bardhan, K., & Liu, K. (2013). Epigenetics and colorectal cancer pathogenesis. *Cancers, 5*(2), 676-713.

Baxter, N., & Rabeneck, L. (2008). New findings about the risks and limitations of colonoscopy used in the early detection of colorectal cancer. *Healthcare Quarterly (Toronto, Ont.), 12*(2), 24-25.

Baxter, N. N., Goldwasser, M. A., Paszat, L. F., Saskin, R., Urbach, D. R., & Rabeneck, L. (2009). Association of colonoscopy and death from colorectal cancer. *Annals of Internal Medicine, 150*(1), 1-8.

Bianchi, P., Laghi, L., Delconte, G., & Malesci, A. (2011). Prognostic Value of Colorectal Cancer Biomarkers. *Cancers, 3*(2), 2080-2105.

Cai, W., Gao, T., Hong, H., & Sun, J. (2008). Applications of gold nanoparticles in cancer nanotechnology. *Nanotechnology, Science and Applications, 1*, 17.

CANSA. (2014). Retrieved from http://www.cansa.org.za/

Cardoso, J., Boer, J., Morreau, H., & Fodde, R. (2007). Expression and genomic profiling of colorectal cancer. *Biochimica et Biophysica Acta (BBA)-Reviews on Cancer, 1775*(1), 103-137.

Causton, B. E. (1984). The choice of resins for electron immunocytochemistry. *Immunolabelling for Electron Microscopy, 1*, 29.

Celis, J. E., Carter, N., Simons, K., Small, J. V., Hunter, T., & Shotton, D. (2005). *Cell Biology, Four-Volume Set: A Laboratory Handbook*: Elsevier Science.

Chanda, N., Kattumuri, V., Shukla, R., Zambre, A., Katti, K., Upendran, A., . . . Casteel, S. W. (2010). Bombesin functionalized gold nanoparticles show in vitro and in vivo cancer receptor specificity. *Proceedings of the National Academy of Sciences, 107*(19), 8760-8765.

Chatterjee, S., Roy, A., Laskar, A., & Swarnakar, S. (2012). Electron Microscopy in the Perspective of Modern Biology: Ultravision and Ultradimension.

Chithrani, B. D., Ghazani, A. A., & Chan, W. C. W. (2006). Determining the size and shape dependence of gold nanoparticle uptake into mammalian cells. *Nano letters, 6*(4), 662-668.

Cho, W.-S., Cho, M., Jeong, J., Choi, M., Han, B. S., Shin, H.-S., . . . Cho, M. (2010). Size-dependent tissue kinetics of PEG-coated gold nanoparticles. *Toxicology and Applied Pharmacology, 245*(1), 116-123. doi: http://dx.doi.org/10.1016/j.taap.2010.02.013

Cho, W.-S., Kim, S., Han, B. S., & Son, W. C. (2009). Comparison of gene expression profiles in mice liver following intravenous injection of 4 and 100nm-sized PEG-coated gold nanoparticles. *Toxicology Letters, 191*(1), 96-102.

Chou, L. Y. T., Ming, K., & Chan, W. C. W. (2011). Strategies for the intracellular delivery of nanoparticles. *Chemical Society Reviews, 40*(1), 233-245.

Chung, D. C. (2000). The genetic basis of colorectal cancer: insights into critical pathways of tumorigenesis. *Gastroenterology, 119*(3), 854-865.

Coetzee, E. (2013). Early detection of colorectal cancer-Colorectal cancer is common and survival is strongly related to the stage of the disease at diagnosis. *Continuing Medical Education, 31*(6), 210-212.

Corpet, D. E., & Pierre, F. (2005). How good are rodent models of carcinogenesis in predicting efficacy in humans? A systematic review and meta-analysis of colon chemoprevention in rats, mice and men. *European Journal of Cancer, 41*(13), 1911-1922.

D'amico, F., & Skarmoutsou, E. (2008). Quantifying immunogold labelling in transmission electron microscopy. *Journal of Microscopy, 230*(1), 9-15.

De Jong, W. H., Hagens, W. I., Krystek, P., Burger, M. C., Sips, A. J., & Geertsma, R. E. (2008). Particle size-dependent organ distribution of gold nanoparticles after intravenous administration. *Biomaterials, 29*(12), 1912-1919.

Deschner, E. E., & Long, F. C. (1977). Colonic neoplasms in mice produced with six injections of 1, 2-dimethylhydrazine. *Oncology, 34*(6), 255-257.

Druckrey, H. (1970). Production of colonic carcinomas by 1, 2-dialkylhydrazines and azoxyalkanes. *Carcinoma of the Colon and Antecedent Epithelium*, 267-279.

El-Brolossy, T. A., Abdallah, T., Mohamed, M. B., Abdallah, S., Easawi, K., Negm, S., & Talaat, H. (2008). Shape and size dependence of the surface plasmon resonance of gold nanoparticles studied by Photoacoustic technique. *The European Physical Journal Special Topics, 153*(1), 361-364.

El-Sayed, I. H., Huang, X., & El-Sayed, M. A. (2006). Selective laser photo-thermal therapy of epithelial carcinoma using anti-EGFR antibody conjugated gold nanoparticles. *Cancer Letters, 239*(1), 129-135.

Encyclopaedia-Britannica.Inc. (2003). Large intestine: mucosa and musculature in humans. Retrieved from http://www.britannica.com/EBchecked/media/68639/Structures-of-the-human-large-intestine-rectum-and-anus-The

Fearon, E. R. (2011). Molecular genetics of colorectal cancer. *Annual Review of Pathology: Mechanisms of Disease, 6*, 479-507.

Fearon, E. R., & Vogelstein, B. (1990). A genetic model for colorectal tumorigenesis. *Cell, 61*(5), 759-767.

Ferlay, J., Shin, H., Bray, F., Forman, D., Mathers, C., & Parkin, D. M. (2010). Estimates of worldwide burden of cancer in 2008: GLOBOCAN 2008. *International Journal of Cancer, 127*(12), 2893-2917.

Ferlay, J., Soerjomataram, I., Ervik, M., Dikshit, R., Eser, S., Mathers, C., . . . Bray, F. (2013). GLOBOCAN 2012 v1.0, Cancer Incidence and Mortality Worldwide: IARC CancerBase (Internet). from Lyon, France: International Agency for Research on Cancer http://globocan.iarc.fr/Default.aspx

Fernandez-Prada, C., Tall, B. D., Elliott, S. E., Hoover, D. L., Nataro, J. P., & Venkatesan, M. M. (1998). Hemolysin-positive enteroaggregative and cell-detaching Escherichia coli strains cause oncosis of human monocyte-derived macrophages and apoptosis of murine J774 cells. *Infection and immunity, 66*(8), 3918-3924.

Feynman, R. P. (1960). There's plenty of room at the bottom. *Engineering and science, 23*(5), 22-36.

Fiala, E. S. (1977). Investigations into the metabolism and mode of action of the colon carcinogens 1, 2-dimethylhydrazine and azoxymethane. *Cancer, 40*(S5), 2436-2445.

Fodde, R. (2002). The APC gene in colorectal cancer. *European Journal of Cancer, 38*(7), 867-871.

Fredericks, E. (2013). Colorectal carcinogenesis : molecular aspects : review. *11*(3), 11-18. http://reference.sabinet.co.za/webx/access/electronic_journals/medgas/medgas_v11_n3_a5.pdf

Frens, G. (1973). Controlled nucleation for the regulation of the particle size in monodisperse gold suspensions. *Nature, 241*(105), 20-22.

García-Bilbao, A., Armañanzas, R., Ispizua, Z., Calvo, B., Alonso-Varona, A., Inza, I., . . . Betanzos, M. (2012). Identification of a biomarker panel for colorectal cancer diagnosis. *BMC Cancer, 12*(1), 43.

Goel, A., & Boland, C. R. (2010). Recent insights into the pathogenesis of colorectal cancer. *Current opinion in gastroenterology, 26*(1), 47.

Goodhew, P. J., Humphreys, J., & Beanland, R. (2000). *Electron Microscopy and Analysis, Third Edition*: CRC Press.

Griffiths, G. (1993). Fixation for fine structure preservation and immunocytochemistry *Fine Structure Immunocytochemistry* (pp. 26-89): Springer.

Grimstone, A. V. (1968). *electron microscope in biology*. London: Hodder & Stoughton Educational; 2nd edition.

Gu, F. X. (2011). Nanotechnology and diagnostic imaging: new advances in contrast agent technology. *Journal of Nanomedicine & Nanotechnology*.

Gupta, R. B., & Kompella, U. B. (2006). *Nanoparticle technology for drug delivery*: Taylor & Francis New York.

Hardcastle, J. D., Chamberlain, J. O., Robinson, M. H. E., Moss, S. M., Amar, S. S., Balfour, T. W., . . . Mangham, C. M. (1996). Randomised controlled trial of faecal-occult-blood screening for colorectal cancer. *The Lancet, 348*(9040), 1472-1477.

Hayat, M. A. (1974). *Principles and techniques of scanning electron microscopy. Biological applications. Volume 1*: Van Nostrand Reinhold Company.

Higby, G. J. (1982). Gold in medicine. *Gold bulletin, 15*(4), 130-140.

Hillyer, J. F., & Albrecht, R. M. (2001). Gastrointestinal persorption and tissue distribution of differently sized colloidal gold nanoparticles. *Journal of pharmaceutical sciences, 90*(12), 1927-1936.

Hirn, S., Semmler-Behnke, M., Schleh, C., Wenk, A., Lipka, J., Schäffler, M., . . . Simon, U. (2011). Particle size-dependent and surface charge-dependent biodistribution of gold nanoparticles after intravenous administration. *European Journal of Pharmaceutics and Biopharmaceutics, 77*(3), 407-416.

Jain, K., El-Sayed, I. H., & El-Sayed, M. A. (2007). Au nanoparticles target cancer. *nano today, 2*(1), 18-29.

Jemal, A., Bray, F., Forman, D., O'Brien, M., Ferlay, J., Center, M., & Parkin, D. M. (2012). Cancer burden in Africa and opportunities for prevention. *Cancer, 118*(18), 4372-4384.

Jiang, J., Oberdörster, G., & Biswas, P. (2009). Characterization of size, surface charge, and agglomeration state of nanoparticle dispersions for toxicological studies. *Journal of Nanoparticle Research, 11*(1), 77-89.

Johns, L. E., & Houlston, R. S. (2001). A systematic review and meta-analysis of familial colorectal cancer risk. *The American Journal of Gastroenterology, 96*(10), 2992-3003.

Johnson, R. L., & Fleet, J. C. (2013). Animal models of colorectal cancer. *Cancer and Metastasis Reviews, 32*(1-2), 39-61.

Jong, W. H. D., Burger, M. C., Verheijen, M. A., & Geertsma, R. E. (2010). Detection of the presence of gold nanoparticles in organs by transmission electron microscopy. *Materials, 3*(9), 4681-4694.

Kanthan, R., Senger, J.-L., & Kanthan, S. C. (2011). Fecal molecular markers for colorectal cancer screening. *Gastroenterology Research and Practice, 2012*.

Keino-Masu, K., Masu, M., Hinck, L., Leonardo, E. D., Chan, S. S.-Y., Culotti, J. G., & Tessier-Lavigne, M. (1996). Deleted in Colorectal Cancer (DCC) Encodes a Netrin Receptor. *Cell, 87*(2), 175-185.

Kelly, K. A., & Jones, D. A. (2003). Isolation of a colon tumor specific binding peptide using phage display selection. *Neoplasia, 5*(5), 437-444.

Kempen, P. J., Thakor, A. S., Zavaleta, C., Gambhir, S. S., & Sinclair, R. (2013). A Scanning Transmission Electron Microscopy Approach to Analyzing Large Volumes of Tissue to Detect Nanoparticles. *Microscopy and Microanalysis, 19*(05), 1290-1297.

Keshav, S., & Bailey, A. (2012). *The gastrointestinal system at a glance* (2 ed.): John Wiley & Sons.

Kettiger, H., Schipanski, A., Wick, P., & Huwyler, J. (2013). Engineered nanomaterial uptake and tissue distribution: from cell to organism. *International Journal of Nanomedicine, 8*, 3255.

Khlebtsov, N., & Dykman, L. (2011). Biodistribution and toxicity of engineered gold nanoparticles: a review of in vitro and in vivo studies. *Chemical Society Reviews, 40*(3), 1647-1671.

Kimling, J., Maier, M., Okenve, B., Kotaidis, V., Ballot, H., & Plech, A. (2006). Turkevich method for gold nanoparticle synthesis revisited. *The Journal of Physical Chemistry B, 110*(32), 15700-15707.

Kirley, S. D., D'Apuzzo, M., Lauwers, G. Y., Graeme-Cook, F., Chung, D. C., & Zukerberg, L. R. (2005). The Cables gene on chromosome 18Q regulates colon cancer progression in vivo. *Cancer biology & therapy, 4*(8), 861-863.

Kitagawa, T., & Ono, K. (1986). Ultrastructure of pancreatic exocrine cells of the rat during starvation. *Histology and Histopathology, 1*(1), 49-57.

Kronborg, O., Fenger, C., Olsen, J., Jørgensen, O. D., & Søndergaard, O. (1996). Randomised study of screening for colorectal cancer with faecal-occult-blood test. *The Lancet, 348*(9040), 1467-1471.

Kühnel, W. (2003). *Color atlas of cytology, histology, and microscopic anatomy*. Germany: Thieme.

Kulkarni, S. A., & Feng, S.-S. (2013). Effects of particle size and surface modification on cellular uptake and biodistribution of polymeric nanoparticles for drug delivery. *Pharmaceutical research, 30*(10), 2512-2522.

Ladner, R. C., Sato, A. K., Gorzelany, J., & de Souza, M. (2004). Phage display-derived peptides as therapeutic alternatives to antibodies. *Drug discovery today, 9*(12), 525-529.

Leslie, A., Carey, F., Pratt, N., & Steele, R. (2002). The colorectal adenoma–carcinoma sequence. *British Journal of Surgery, 89*(7), 845-860.

Li, J.-L., Wang, L., Liu, X.-Y., Zhang, Z.-P., Guo, H.-C., Liu, W.-M., & Tang, S.-H. (2009). In vitro cancer cell imaging and therapy using transferrin-conjugated gold nanoparticles. *Cancer letters, 274*(2), 319-326.

Liou, W., Geuze, H. J., & Slot, J. W. (1996). Improving structural integrity of cryosections for immunogold labeling. *Histochemistry and cell biology, 106*(1), 41-58.

Lipka, J., Semmler-Behnke, M., Sperling, R. A., Wenk, A., Takenaka, S., Schleh, C., . . . Kreyling, W. G. (2010). Biodistribution of PEG-modified gold nanoparticles following intratracheal instillation and intravenous injection. *Biomaterials, 31*(25), 6574-6581.

Littlejohn, C., Hilton, S., Macfarlane, G. J., & Phull, P. (2012). Systematic review and meta-analysis of the evidence for flexible sigmoidoscopy as a screening method for the prevention of colorectal cancer. *British Journal of Surgery, 99*(11), 1488-1500.

Loqman, M. Y., Bush, P. G., Farquharson, C., & Hall, A. C. (2010). A cell shrinkage artefact in growth plate chondrocytes with common fixative solutions: importance of fixative osmolarity for maintaining morphology. *European Cells and Materials, 14*(19), 214-227.

Lucocq, J. M., & Gawden-Bone, C. (2010). Quantitative assessment of specificity in immunoelectron microscopy. *Journal of Histochemistry & Cytochemistry, 58*(10), 917-927.

Lund, T., Callaghan, M. F., Williams, P., Turmaine, M., Bachmann, C., Rademacher, T., . . . Bayford, R. (2011). The influence of ligand organization on the rate of uptake of gold nanoparticles by colorectal cancer cells. *Biomaterials, 32*(36), 9776-9784.

Luo, Y., Sun, W., Gu, Y., Wang, G., & Fang, N. (2010). Wavelength-dependent differential interference contrast microscopy: multiplexing detection using nonfluorescent nanoparticles. *Analytical Chemistry, 82*(15), 6675-6679.

Magee, W., Sheek, M., & Sagik, B. (1958). Methods of harvesting mammalian cells grown in tissue culture. *Experimental Biology and Medicine, 99*(2), 390-392.

Majno, G., & Joris, I. (1995). Apoptosis, oncosis, and necrosis. An overview of cell death. *The American Journal of Pathology, 146*(1), 3.

Mallidi, S., Larson, T., Tam, J., Joshi, P. P., Karpiouk, A., Sokolov, K., & Emelianov, S. (2009). Multiwavelength photoacoustic imaging and plasmon resonance coupling of gold nanoparticles for selective detection of cancer. *Nano Letters, 9*(8), 2825-2831.

Martin, M., Martin, F., Michiels, R., Bastien, H., Justrabo, E., Bordes, M., & Viry, B. (1973). An experimental model for cancer of the colon and rectum. *Digestion, 8*(1), 22-34.

Mayhew, T. (2009). Quantifying immunogold localization patterns on electron microscopic thin sections of placenta: recent developments. *Placenta, 30*(7), 565-570.

Mazyambe, M. K. (2013). *Evaluating the specificty of cancer cell targeting peptides for applications in cancer diagnostics* (Unpublished master's thesis Thesis), University of the Western Cape.

McNeil, S. E. (2005). Nanotechnology for the biologist. *Journal of Leukocyte Biology, 78*(3), 585-594.

Miller, B. V., & Lines, R. W. (1988). Recent advances in particle size measurements: a critical review. *Critical Reviews in Analytical Chemistry, 20*(2), 75-116.

Mironava, T., Hadjiargyrou, M., Simon, M., Jurukovski, V., & Rafailovich, M. H. (2010). Gold nanoparticles cellular toxicity and recovery: effect of size, concentration and exposure time. *Nanotoxicology, 4*(1), 120-137.

Mohamed Anwar, K., & Halim, A. (2012). The Influence of Size and Exposure Duration of Gold Nanoparticles on Gold Nanoparticles Levels in Several Rat Organs In vivo. *Journal of Cell Science & Therapy*.

Morais, T., Soares, M. E., Duarte, J. A., Soares, L., Maia, S., Gomes, P., . . . Bastos, M. d. L. (2012). Effect of surface coating on the biodistribution profile of gold nanoparticles in the rat. *European Journal of Pharmaceutics and Biopharmaceutics, 80*(1), 185-193.

Morin, P. J., Sparks, A. B., Korinek, V., Barker, N., Clevers, H., Vogelstein, B., & Kinzler, K. W. (1997). Activation of β-catenin-Tcf signaling in colon cancer by mutations in β-catenin or APC. *Science, 275*(5307), 1787-1790.

Mühlfeld, C., Rothen-Rutishauser, B., Vanhecke, D., Blank, F., Gehr, P., & Ochs, M. (2007). Visualization and quantitative analysis of nanoparticles in the respiratory tract by transmission electron microscopy. *Part Fibre Toxicol, 4*(11), 1-17.

Nativo, P., Prior, I. A., & Brust, M. (2008). Uptake and intracellular fate of surface-modified gold nanoparticles. *ACS nano, 2*(8), 1639-1644.

Neufert, C., Becker, C., & Neurath, M. F. (2007). An inducible mouse model of colon carcinogenesis for the analysis of sporadic and inflammation-driven tumor progression. *Nature PJournal of Zhejiang University SCIENCE Brotocols, 2*(8), 1998-2004.

Newman, G. R., & Hobot, J. A. (1999). Resins for combined light and electron microscopy: a half century of development. *The Histochemical Journal, 31*(8), 495-505.

Newman, G. R., Jasani, B., & Williams, E. D. (1982). The preservation of ultrastructure and antigenicity. *Journal of Microscopy, 127*(3), RP5-RP6.

Newman, G. R., Jasani, B., & Williams, E. D. (1983). A simple post-embedding system for the rapid demonstration of tissue antigens under the electron microscope. *The Histochemical Journal, 15*(6), 543-555.

Ng, C. T., Li, J. J., Perumalsamy, R., Watt, F., Yung, L. Y. L., & Bay, B. H. (2010). Localizing cellular uptake of nanomaterials in vitro by transmission electron microscopy. *Microscopy: Science, Technology, Applications and Education, 1*, 316-320.

O'Connell, J. B., Maggard, M. A., & Ko, C. Y. (2004). Colon cancer survival rates with the new American Joint Committee on Cancer sixth edition staging. *Journal of the National Cancer Institute, 96*(19), 1420-1425.

Pancione, M., Remo, A., & Colantuoni, V. (2012). Genetic and epigenetic events generate multiple pathways in colorectal cancer progression. *Pathology Research International, 2012*.

Papasani, M. R., Wang, G., & Hill, R. A. (2012). Gold nanoparticles: the importance of physiological principles to devise strategies for targeted drug delivery. *Nanomedicine: Nanotechnology, Biology and Medicine, 8*(6), 804-814.

Patra, C. R., Bhattacharya, R., Mukhopadhyay, D., & Mukherjee, P. (2010). Fabrication of gold nanoparticles for targeted therapy in pancreatic cancer. *Advanced Drug Delivery Reviews, 62*(3), 346-361.

Patri, A. K., Myc, A., Beals, J., Thomas, T. P., Bander, N. H., & Baker, J. R. (2004). Synthesis and in vitro testing of J591 antibody-dendrimer conjugates for targeted prostate cancer therapy. *Bioconjugate Chemistry, 15*(6), 1174-1181.

Perše, M., & Cerar, A. (2005). The dimethylhydrazine induced colorectal tumours in rat-experimental colorectal carcinogenesis. *Radiology and Oncology, 39*(1).

Perše, M., & Cerar, A. (2012). Dextran sodium sulphate colitis mouse model: traps and tricks. *BioMed Research International, 2012*.

Philimonenko, V. V., Janacek, P., & Hozak, P. (2002). LR White is preferable to Unicryl for immunogold detection of fixationsensitive nuclear antigens. *European Journal of Histochemistry, 46*(4), 359-364.

Pino, M. S., & Chung, D. C. (2010). The chromosomal instability pathway in colon cancer. *Gastroenterology, 138*(6), 2059-2072.

Pitule, P., Čedíková, M., Třeška, V., Králíčková, M., & Liška, V. (2013). Assessing colorectal cancer heterogeneity: one step closer to tailored medicine. *Journal of Applied Biomedicine, 11*(3), 115-129.

Popovtzer, R., Agrawal, A., Kotov, N. A., Popovtzer, A., Balter, J., Carey, T. E., & Kopelman, R. (2008). Targeted gold nanoparticles enable molecular CT imaging of cancer. *Nano Letters, 8*(12), 4593-4596.

Pritchard, C. C., & Grady, W. M. (2010). Colorectal cancer molecular biology moves into clinical practice. *Gut*, gut. 2009.206250.

Proskuryakov, S. Y. a., Konoplyannikov, A. G., & Gabai, V. L. (2003). Necrosis: a specific form of programmed cell death? *Experimental Cell Research, 283*(1), 1-16. doi: http://dx.doi.org/10.1016/S0014-4827(02)00027-7

Raschke, G., Brogl, S., Susha, A., Rogach, A., Klar, T., Feldmann, J., . . . Nichtl, A. (2004). Gold nanoshells improve single nanoparticle molecular sensors. *Nano Letters, 4*(10), 1853-1857.

Ravnik-Glavač, M., Cerar, A., & Glavač, D. (2000). Animal model in the study of colorectal carcinogenesis. *Pflügers Archiv, 440*(1), r055-r057.

Reuveni, T., Motiei, M., Romman, Z., Popovtzer, A., & Popovtzer, R. (2011). Targeted gold nanoparticles enable molecular CT imaging of cancer: an in vivo study. *International journal of nanomedicine, 6*, 2859.

Rex, D. K., Cutler, C. S., Lemmel, G. T., Rahmani, E. Y., Clark, D. W., Helper, D. J., . . . Mark, D. G. (1997). Colonoscopic miss rates of adenomas determined by back-to-back colonoscopies. *Gastroenterology, 112*(1), 24-28.

Robertis, M. D., Massi, E., Poeta, M. L., Carotti, S., Morini, S., Cecchetelli, L., . . . Fazio, V. M. (2011). The AOM/DSS murine model for the study of colon carcinogenesis: From pathways to diagnosis and therapy studies. *Journal of Carcinogenesis, 10*(1), 9.

Rosenberg, D. W., Giardina, C., & Tanaka, T. (2009). Mouse models for the study of colon carcinogenesis. *Carcinogenesis, 30*(2), 183-196.

Rosner, G., & Strul, H. (2014). Should Microsatellite Instability Be Tested in All Cases of Colorectal Cancer? *Current Colorectal Cancer Reports, 10*(1), 27-35.

Rustgi, A. K. (2007). The genetics of hereditary colon cancer. *Genes & development, 21*(20), 2525-2538.

Ryan, U. S., & Hart, M. A. (1986). Electron microscopy of endothelial cells in culture: I. Transmission electron microscopy. *Journal of Tissue Culture Methods, 10*(1), 31-33.

Sabatini, D. D., Miller, F., & Barrnett, R. J. (1964). Aldehyde fixation for morphological and enzyme histochemical studies with the electron microscope. *Journal of Histochemistry & Cytochemistry, 12*(2), 57-71.

Sahoo, S. K., Parveen, S., & Panda, J. J. (2007). The present and future of nanotechnology in human health care. *Nanomedicine: Nanotechnology, Biology and Medicine, 3*(1), 20-31.

Sameer, A. S. (2013). Colorectal cancer: a researcher's perspective of the molecular angel's gone eccentric in the Vale of Kashmir. *Tumor Biology, 34*(3), 1301-1315.

Sapra, P., & Allen, T. M. (2002). Internalizing antibodies are necessary for improved therapeutic efficacy of antibody-targeted liposomal drugs. *Cancer Research, 62*(24), 7190-7194.

Scholefield, J. H., Moss, S., Sufi, F., Mangham, C. M., & Hardcastle, J. D. (2002). Effect of faecal occult blood screening on mortality from colorectal cancer: results from a randomised controlled trial. *Gut, 50*(6), 840-844.

Schrand, A. M., Schlager, J. J., Dai, L., & Hussain, S. M. (2010). Preparation of cells for assessing ultrastructural localization of nanoparticles with transmission electron microscopy. *Nature Protocols, 5*(4), 744-757.

Shadidi, M., & Sioud, M. (2003). Selective targeting of cancer cells using synthetic peptides. *Drug Resistance Updates, 6*(6), 363-371.

Shi, X., Li, D., Xie, J., Wang, S., Wu, Z., & Chen, H. (2012). Spectroscopic investigation of the interactions between gold nanoparticles and bovine serum albumin. *Chinese Science Bulletin, 57*(10), 1109-1115.

Skepper, J. N., & Powell, J. M. (2008). Immunogold staining of London Resin (LR) White sections for transmission electron microscopy (TEM). *Cold Spring Harbor Protocols, 2008*(6), pdb. prot5016.

Sokolov, K., Follen, M., Aaron, J., Pavlova, I., Malpica, A., Lotan, R., & Richards-Kortum, R. (2003). Real-time vital optical imaging of precancer using anti-epidermal growth factor receptor antibodies conjugated to gold nanoparticles. *Cancer Research, 63*(9), 1999-2004.

Sonavane, G., Tomoda, K., Sano, A., Ohshima, H., Terada, H., & Makino, K. (2008). In vitro permeation of gold nanoparticles through rat skin and rat intestine: Effect of particle size. *Colloids and Surfaces B: Biointerfaces, 65*(1), 1-10.

Sperling, R. A., Gil, P. R., Zhang, F., Zanella, M., & Parak, W. J. (2008). Biological applications of gold nanoparticles. *Chemical Society Reviews, 37*(9), 1896-1908.

Suzuki, R., Kohno, H., Sugie, S., & Tanaka, T. (2005). Dose-dependent promoting effect of dextran sodium sulfate on mouse colon carcinogenesis initiated with azoxymethane.

Takahashi, M., Mutoh, M., Kawamori, T., Sugimura, T., & Wakabayashi, K. (2000). Altered expression of β-catenin, inducible nitric oxide synthase and cyclooxygenase-2 in azoxymethane-induced rat colon carcinogenesis. *Carcinogenesis, 21*(7), 1319-1327.

Takizawa, T., Anderson, C. L., & Robinson, J. M. (2003). A new method to enhance contrast of ultrathin cryosections for immunoelectron microscopy. *Journal of Histochemistry & Cytochemistry, 51*(1), 31-39.

Tan, C., & Du, X. (2012). KRAS mutation testing in metastatic colorectal cancer. *World journal of gastroenterology: WJG, 18*(37), 5171.

Tanaka, T., Kohno, H., Suzuki, R., Yamada, Y., Sugie, S., & Mori, H. (2003). A novel inflammation-related mouse colon carcinogenesis model induced by azoxymethane and dextran sodium sulfate. *Cancer Science, 94*(11), 965-973.

Tanaka, T., Tanaka, M., Tanaka, T., & Ishigamori, R. (2010). Biomarkers for colorectal cancer. *International Journal of Molecular Sciences, 11*(9), 3209-3225.

Thaker, A. I., Shaker, A., Rao, M. S., & Ciorba, M. A. (2012). Modeling colitis-associated cancer with azoxymethane (AOM) and dextran sulfate sodium (DSS). *Journal of visualized experiments: JoVE*(67).

Thakor, A., Jokerst, J., Zavaleta, C., Massoud, T., & Gambhir, S. (2011). Gold nanoparticles: a revival in precious metal administration to patients. *Nano Letters, 11*(10), 4029-4036.

Tiwari, P. M., Vig, K., Dennis, V. A., & Singh, S. R. (2011). Functionalized gold nanoparticles and their biomedical applications. *Nanomaterials, 1*(1), 31-63.

Treuel, L., Jiang, X., & Nienhaus, G. U. (2013). New views on cellular uptake and trafficking of manufactured nanoparticles. *Journal of The Royal Society Interface, 10*(82), 20120939.

Turkevich, J., Stevenson, P. C., & Hillier, J. (1951). A study of the nucleation and growth processes in the synthesis of colloidal gold. *Discussions of the Faraday Society, 11*(0), 55-75. doi: 10.1039/DF9511100055

Venkatachalam, R., Ligtenberg, M. J., Hoogerbrugge, N., de Bruijn, D. R., Kuiper, R. P., & Geurts van Kessel, A. (2010). The epigenetics of (hereditary) colorectal cancer. *Cancer Genetics and Cytogenetics, 203*(1), 1-6.

Verlander, J. W. (1998). Normal ultrastructure of the kidney and lower urinary tract. *Toxicologic pathology, 26*(1), 1-17.

Wang, J.-J., Liu, Y., Zheng, Y., Liao, K.-X., Lin, F., Wu, C.-T., . . . Yao, X.-Q. (2012). Screening Peptides Binding Specifically to Colorectal Cancer Cells from a Phage Random Peptide Library. *Asian Pacific Journal of Cancer Prevention, 13*, 377-381.

Wang, M., & Thanou, M. (2010). Targeting nanoparticles to cancer. *Pharmacological Research, 62*(2), 90-99.

Wang, X.-F., Birringer, M., Dong, L.-F., Veprek, P., Low, P., Swettenham, E., . . . Wu, K. (2007). A peptide conjugate of vitamin E succinate targets breast cancer cells with high ErbB2 expression. *Cancer Research, 67*(7), 3337-3344.

Wang, X. Z., Liu, L., Li, R. F., Tweedie, R. J., Primrose, K., Corbett, J., & McNeil-Watson, F. K. (2009). Online characterisation of nanoparticle suspensions using dynamic light scattering, ultrasound spectroscopy and process tomography. *Chemical Engineering Research and Design, 87*(6), 874-884.

Wang, Z. L. (2000). Transmission electron microscopy of shape-controlled nanocrystals and their assemblies. *The Journal of Physical Chemistry B, 104*(6), 1153-1175.

Wickens, N. J. (2012). *Histopathological changes in male wistar rats maintained on a water-based Sutherlandia Frutescence extract.* (Doctor Technologiae), Nelson Mandela Metropolitan University.

Willets, K. A., & Van Duyne, R. P. (2007). Localized surface plasmon resonance spectroscopy and sensing. *Annu. Rev. Phys. Chem., 58*, 267-297.

Wu, J. S., Kim, A. M., Bleher, R., Myers, B. D., Marvin, R. G., Inada, H., . . . Dravid, V. P. (2013). Imaging and elemental mapping of biological specimens with a dual-EDS dedicated scanning transmission electron microscope. *Ultramicroscopy, 128*(0), 24-31.

Wu, P., Leinonen, J., Koivunen, E., Lankinen, H., & Stenman, U. H. (2000). Identification of novel prostate-specific antigen-binding peptides modulating its enzyme activity. *European Journal of Biochemistry, 267*(20), 6212-6220.

Yin Win, K., & Feng, S.-S. (2005). Effects of particle size and surface coating on cellular uptake of polymeric nanoparticles for oral delivery of anticancer drugs. *Biomaterials, 26*(15), 2713-2722.

Yoshimi, K., Tanaka, T., Takizawa, A., Kato, M., Hirabayashi, M., Mashimo, T., . . . Kuramoto, T. (2009). Enhanced colitis-associated colon carcinogenesis in a novel Apc mutant rat. *Cancer Science, 100*(11), 2022-2027.

Yu, M. K., Park, J., & Jon, S. (2012). Targeting strategies for multifunctional nanoparticles in cancer imaging and therapy. *Theranostics, 2*(1), 3.

Zhang, X.-D., Wu, D., Shen, X., Liu, P.-X., Yang, N., Zhao, B., . . . Fan, F.-Y. (2011). Size-dependent in vivo toxicity of PEG-coated gold nanoparticles. *International journal of nanomedicine, 6*, 2071.

Zhao, P., Li, N., & Astruc, D. (2013). State of the art in gold nanoparticle synthesis. *Coordination Chemistry Reviews, 257*(3), 638-665.

APPENDIX

• PO Box 77000 • Nelson Mandela Metropolitan University
• Port Elizabeth • 6031 • South Africa • www.nmmu.ac.za

Nelson Mandela Metropolitan University
for tomorrow

Chairperson of the Research Ethics Committee (Animal)
NMMU
Tel . +27 (0)41 504-4273 Fax. +27 (0)41 504-2814

Ref: [A13-SCI-ZOO-013/Approval]

Contact person: Mrs U Spies

22 November 2013

Prof S Roux
NMMU
Faculty of Science
Department of Biochemistry and Microbiology
12-03-03
South Campus

Dear Prof Roux

EVALUATION OF GOLD NANOPARTICLES FOR THE DIAGNOSIS OF COLORECTAL CANCER

PRP: Prof S Roux
PI: Ms L Calmcross

We take pleasure in informing you that the above-mentioned application submitted to the Research Ethics Committee (Animal) for ethics approval, was approved by the Committee.

The ethics clearance reference number is **A13-SCI-ZOO-013.**

Ethics approval remains **valid for three years**, provided that the approved protocols and conditions remain unchanged and that the applicant agrees to regular monitoring (video recordings if necessary where field work is involved) by the RECA for the duration of the project. At the end of the third year, you will have to affirm that the project is complete, or reapply for ethics approval. You will receive the appropriate reminder and documentation each year well in time for any applicable deadline.

Please inform your co-investigators of the outcome. We wish you well with the project.

Yours sincerely

Dr G Dealtry
Chairperson: Research Ethics Committee (Animal)

cc: Department of Research Capacity Development
Faculty Officer: Science

/us